The complementarity of luminescence dating methods illustrated on the Mousterian sequence of the Roc de Marsal: A series of reindeer-dominated, Quina Mousterian layers dated to MIS 3

Guillaume Guérin, Marine Frouin, Joséphine Tuquoi, K.J. Thomsen, Paul Goldberg, Vera Aldeias, Christelle Lahaye, Norbert Mercier, Pierre Guibert, Mayank Jain, et al.

The complementarity of luminescence dating methods illustrated on the Mousterian sequence of the Roc de Marsal: A series of reindeer-dominated, Quina Mousterian layers dated to MIS 3

Guillaume Guérin[1], Marine Frouin[2,1], Joséphine Tuquoi[1], Kristina J. Thomsen[3], Paul Goldberg[4,5,6], Vera Aldeias[7], Christelle Lahaye[1], Norbert Mercier[1], Pierre Guibert[1], Mayank Jain[3], Dennis Sandgathe[8], Shannon P. McPherron[7], Alain Turq[9,10], Harold L. Dibble[11,12,7].

Abstract

Located in southwest France, Roc de Marsal is a cave with a rich Mousterian stratigraphic sequence. The lower part of the sequence (Layers 9-5) are characterized by assemblages dominated by Levallois lithic technology associated with composite faunal spectra (including red deer, roe deer and reindeer) that shows a gradual increase in the frequency of reindeer. The top of the sequence (Layers 4-2) are characterised instead by Quina lithic technology (both in terms of technology and typology) with the faunal remains dominated by reindeer. Roc de Marsal thus provides a very interesting case study to place behavioural changes in a context of changing climates and environments in western Europe during the late Pleistocene. To link the occupations at Roc de Marsal with global and regional climatic conditions known independently, a robust chronology is needed. With this aim in mind, we applied three luminescence dating methods (TL, OSL and IRSL) on different minerals (flint, quartz and K-feldspar extracts). Here the results of two of these methods are presented in detail (TL and OSL) and compared with preliminary IRSL data. At Roc de Marsal, a comparison of methods was necessary to overcome a complex sedimentary history, with very heterogeneous dose rate distributions, both at the beta (mm) and gamma (dm) dose rate scales. The results indicate that the lower Levallois layers are dated to ~65-70 ka, while overlying Quina layers are dated to ~49 ka. These ages for the lower layers fit well with some models that place mixed faunal assemblages in the initial MIS 4; however, while the Quina ages overlap with several other Quina assemblages from the region, they place the reindeer dominated fauna well after the peak cold of MIS 4 and suggest a more extended and complex period of contemporaneous lithic techno-complexes than posited by some current models.

Keywords

Middle Palaeolithic variability; Quina Mousterian; Luminescence dating methods (TL, OSL, IRSL); Single Grain OSL; dose rate heterogeneities.

1. Introduction

Though the terms of the debate have shifted in fifty plus years from varying proportions of retouched tool types to varying proportions of blank production techniques, the sources of Mousterian variability are still very much debated. Despite the changing terms, an emerging consensus among some researchers is that, in fact, Mellars (1967, 1969, 1996) was essentially correct in his observation that the lithic and faunal assemblages of stratified Late Pleistocene Mousterian sites in southwest France vary in a systematic fashion such that a cultural-historical framework can be constructed from the combined sequences (*e.g.* Jaubert, 2011; Discamps *et al.,* 2011; Morin *et al.,* 2014). In the 1980s, Mellars and Grün (1991) and others (*e.g.* Valladas *et al.,* 1986) saw an opportunity in the development of Thermoluminescence (TL) and Electron Spin Resonance (ESR) dating techniques to apply an independent test to this cultural-historical model, but it has only been in the last decade or more with the addition of OSL dating and improved techniques for radiocarbon dating that the number of dated layers and sites has increased to the point of being able to evaluate the model. While in many ways the dates do tend to support many aspects of the cultural-historical framework, there remain some, sometimes significant, exceptions, and these apparent exceptions have then become the focus of debates, for instance, over the limits in precision of chronometric methods versus sequences built on stratigraphic observations, over how the techno-complex attribution of particular assemblages has been measured or defined, and over the strengths and weaknesses of other types of chronological proxies such as sedimentology, pollen, and fauna.

In this context, one of the reasons we re-opened the southwest France cave site of Roc de Marsal was to obtain a set of radiometric ages on the sequence. This sequence (developed on about 1 to 1.5 m of stratigraphy) can be roughly divided into two blocks: the upper part of the sequence (Layers 2, 3 and 4) yielded an extremely rich Quina Mousterian lithic industry associated with almost exclusive *Rangifer tarandus* remains (Guérin *et al.*, 2012a; Castel *et al.*, this issue), while the lower part of the sequence (Layers 5 to 9) is dominated by a Mousterian with Levallois technology. In addition to very-well preserved combustion features associated with the basal occupations (Sandgathe *et al.*, 2011; Aldeias *et al.*, 2012), these layers exhibit faunal remains of *Rangifer tarandus*, but also *Capreolus capreolus* and *Cervus sp*.

A previous attempt to define the chronology of the Roc de Marsal sequence was published by Guérin *et al.* (2012a). TL on heated flint and sedimentary quartz, and multi-grain, fine grain OSL on sedimentary quartz were used to provide ages for the sequence. On the one hand, Guérin *et al.* (2012a) concluded that their OSL ages were affected either by (i) inaccurate beta dose rate measurements due to heterogeneities in the spatial distribution of radioelements, or by (ii) signal resetting problems possibly arising from the *in situ* degradation of bedrock fragments and subsequent release of quartz grains that would not have been exposed to sunlight before burial (or by a combination of both problems). As a result, the OSL ages were not deemed accurate and Guérin *et al.* (2012a) suggested that a more comprehensive single grain OSL study, together with adequate statistical modelling, might improve the OSL chronology of the sequence. On the other hand, TL ages – despite some unavoidable scatter due to highly variable gamma dose rates over tens of centimetres in sediments, especially close to the bedrock or to collapsed limestone blocks – were deemed accurate by the authors. These ages suggested MIS 4 occupations for the lower layers (Layers 7, 8 and 9). These ages fit well with data assembled by Discamps *et al.* (2011) which show that composite spectra including red deer, roe deer and also reindeer could correspond to a period around 70 ka or MIS 4.

For the upper layers and in particular for the Quina Mousterian occupation layers, the scarcity of burnt flints studied by Guérin *et al.* (2012a) precluded them from drawing firm

conclusions: only two ages for Layer 4 were obtained (61 ± 7 and 45 ± 4 ka) leaving the possibility to attribute this layer either to MIS 4 (assuming that the younger of the two ages is affected by an unrecognized source of error) or to MIS 3 (both ages are consistent with this hypothesis, but the evidence is weak). An MIS 3 age would overlap well with the relatively few published ages for Quina Mousterian (see the review in Guibert *et al.*, 2008). One clear exception is the TL ages from a portion of the thick Quina deposits at Jonzac which, despite very large uncertainties, most likely indicate MIS 4 occupations (Richter *et al.*, 2013a). However, late ages such as these also strongly suggest that Quina Mousterian must overlap with other types of Mousterian, most notably the Mousterian of Acheulean Tradition (MTA; McPherron *et al.,* 2012; Soressi *et al.,* 2013). On the other hand, as the Roc de Marsal Quina assemblages are dominated by reindeer, this would fit better in a late MIS 4 or early MIS 3 paleoenvironemental context (Discamps *et al.* 2011) and would be a better fit with the cultural-historical framework by avoiding chronological overlap with other late Mousterian techno-complexes.

Thus, the present study addresses two points raised by Guérin *et al.* (2012a). First, single grain OSL was measured with the aims of understanding and resolving shortcomings of the previous multi-grain OSL results. Second, an additional set of heated flints from Layers 2 to 6 was studied to complete the previous TL dataset and refine the chronology of particularly the Quina Mousterian layers at Roc de Marsal. These two new datasets will also be viewed in the light of preliminary IRSL measurements (Frouin, 2014). For a regional map, a site map and the stratigraphy investigated in the present study, the reader is referred to Figs. 1, 2 and 3 of Guérin *et al.* (2012a), respectively.

2. Materials and methods

Sixteen flint samples showing traces of heating (pot lids, colour alteration) and recovered from Layers 2 to 6 were tested for TL dating. For the single grain OSL measurements, eight sediment samples from the previous study (Guérin *et al.*, 2012a) were selected with a special focus on the Quina layers (samples Bdx 13401, -402, -408, -409 come from Layers 2-4, *cf.* Table 3), but also on samples from combustion features (13394, -396 and -397, all coming from Layer 9). Indeed these samples were heated to temperatures of several hundred Celsius degrees in the past, and as a result should not suffer from signal resetting problems. These samples were thus selected to help interpret the results of the unheated sediment samples.

2.1. TL on heated flints

All TL measurements were performed with a Lexsyg Research Instrument equipped with a combination of 3 mm of Schott-KG 3 filter and 5 mm of AHF BrightLine HC 475/50 interference filter, to measure emissions around 475 nm (this detection window slightly differs from that used by Guérin *et al.*, 2012a; this choice was driven by optimal signal to noise ratio). A Hamamatsu H7360-02 photomultiplier tube was used to detect the TL signals. A series of tests performed on a small fraction of each flint led to discard of four of the sixteen samples; the twelve others showed a well-defined natural TL peak around 370 °C (with a heating rate of 4°C/s), indicating that they were sufficiently heated in the past to reset their TL signal. However, of these twelve, only six samples were large enough to mechanically remove the outer 2 mm using a low-speed, water-cooled saw, to eliminate any parts irradiated by external beta radiations. The six selected flints were gently crushed to isolate the 100-160 µm fraction. After treatment with HCl and H_2O_2, the samples were rinsed, dried and aliquots of ~8 mm diameter were mounted with silicon oil on stainless steel cups. The $^{90}Sr/^{90}Y$ beta source was calibrated using gamma dosed flint samples, with a measured dose rate of (6.86 ± 0.14) 10^{-2} Gy/s. A Multiple Aliquot Additive Dose protocol similar as that used by Guérin *et al.* (2012a) was used; signal resetting to build second glow curves was performed by heating natural

material to 350°C for 1 hour. For each added or regenerated dose, 4 aliquots were measured. Fig. 1 shows typical TL glow curves and the corresponding additive and regenerated dose response curves for sample Bdx 16773. For additional details about the protocol, the reader is referred to Guérin *et al.* (2012a).

2.2. Quartz single grain OSL

The OSL from single grains of quartz was measured using a Risø TL/OSL reader (DA 20) fitted with a single grain attachment (Duller *et al.*, 1999; Bøtter-Jensen *et al.*, 2000). The grains were loaded into aluminium single-grain discs; each disc contains 100 holes 300 µm in diameter and 300 µm deep, drilled on a 10 x 10 rectangular grid with 600 µm spacing between hole centres. A green laser (532 nm) was used with a 7.5 mm Hoya U-340 detection filter. To check that only one grain was loaded into each hole, the single grain discs were visually inspected using a microscope before measurement. The spatial homogeneity of the ^{90}Sr/^{90}Y beta source (ID 155, produced prior to 2000) used for the single grain measurements presented here was determined using radiochromic film (GAFCHROMIC EBT2) and the coefficient of variation was found to be ~5%, which is unlikely to affect our dose distributions significantly. Using the approach developed by Lapp *et al.* (2012) to correct for spatial beta source heterogeneity, no significant changes in dose or scatter in our dose distributions could be detected, which is consistent with the observations of Sim *et al.* (2014) for the same source. Thus, the laboratory beta dose rate employed in further single grain calculations is based on the average over the whole disc.

The Single Aliquot Regenerative dose protocol (SAR protocol; Murray and Wintle, 2000) employed in these single grain measurements included a post-IR green signal (1 s stimulation with green laser at 125 °C following a 40 s stimulation with IR diodes at 125 °C) and is similar as that used by Guérin *et al.* (2015a). A preheat at 260 °C for ten seconds and cutheat at 220 °C were used before, respectively, regenerated (and natural) and test dose signals. A preheat plateau test was performed on natural samples and did not show variations in D_e values (data not shown). The net signal used in D_e calculations was derived from the sum of the OSL in the first 0.05 s of stimulation less a background signal (time average of the last 0.2 s). Dose response curves were measured up to 220 Gy for each individual grain. These were fitted with a single saturating exponential function of the form $y = A\,(1 - \exp(D / D_0))$ where y is the sensitivity corrected OSL signal, D is the dose, A is the saturation level of the sensitivity-corrected OSL signal and D_0 is the dose at which y is at 63 % of the saturation level.

Appropriate analysis of single grain OSL has been the subject of quite intense debate in the OSL community over the last 15 years. Indeed, the sensitivity of quartz grains is highly variable; in one sample, the OSL response to a fixed dose varies by several orders of magnitude from grain to grain. This led to the need for statistical modelling of single grain OSL data, even for samples unaffected by post-depositional mixing and insufficient exposure to sunlight before burial (Galbraith *et al.*, 1999; Combès *et al.*, 2015). The first stage of single grain data analysis consists of selecting the grains whose signals are used for statistical modelling. Beyond the obvious selection of grains emitting light (here we selected grains for which the uncertainty on the first test dose signal was less than 20%, following *e.g.* Thomsen *et al.*, 2003), some authors argue for strict rejection criteria (*e.g.*, Yoshida *et al.*, 2000; Jacobs *et al.*, 2006, and references therein) based essentially on the response of grains to a number of quality-insurance tests of the SAR protocol, such as recycling, recuperation and IR depletion ratios (Murray and Wintle, 2000; 2003; Wintle and Murray, 2006; Duller, 2003). Others have reported that the main effect of such rejection criteria is to reduce the number of selected grains with negligible effects on the estimated D_e and overdispersion (OD) parameters, which might thus lead to a loss of robustness in the final results (*e.g.*, Thomsen *et al.*, 2012; Guérin *et al.*, 2015a;

Geach *et al.*, 2015; Hansen *et al.*, 2015; Kristensen *et al.*, 2015; Zhao *et al.*, 2015; Thomsen *et al.*, 2016).

Other selection criteria have been proposed, among which the D_0 selection criterion (Thomsen *et al.*, 2016) and the Fast Ratio (Madsen *et al.*, 2009; Durcan and Duller, 2011). The former of the two is applied to remove early saturating grains that would bias D_e distributions since, with such grains, only the lower part of the dose distributions can be retrieved. For example, it will not be possible to accurately measure a dose of 100 Gy using a grain with a dose response curve characterised by a D_0 value of say 25 Gy, as the OSL signal will be too close to its asymptotic value to give a bounded dose estimate. Applying a rejection criterion where all dose estimates are less than 2 D_0 is inherently a dose dependent rejection criterion which is undesirable. Instead we have tested the effect of rejecting individual dose estimates based solely on their D_0 value for different values of D_0 and evaluated the effect of this selection criterion (D_0>x) with two parameters: the fraction of grains in saturation (which should be zero when working with well-bleached populations of grains showing an adequate OSL dynamic range), and the average equivalent dose as a function of x (a plateau is supposed to indicate an acceptable range of x values). The Fast Ratio criterion was developed to select only those grains for which the quartz OSL signal is dominated by the fast component. However, Thomsen *et al.* (2015) showed by studying single grain OSL with an EM–CCD camera that the variability in the decay rates of OSL signals is predominantly an artefact of the laser stimulation system, rather than a reflection of variable intensities in fast versus medium components. Nonetheless, Thomsen *et al.* (2016) found an improvement in accuracy of 8 ± 3 % (average of 4 samples) when only including grains with the largest Fast Ratio values, but this was at a cost of rejecting ~90 % of the otherwise accepted grain population. As a result, we have not investigated the effect of the fast ratio selection on our datasets.

Another current subject of debate in the community is age, or rather dose modelling. The most commonly used approach for well-bleached samples, and single dose populations as in dose recovery experiments, is the Central Age Model (Galbraith *et al.*, 1999). However, several studies have recently argued against this model, based on different strands of evidence. Thomsen *et al.* (2016) and Guérin *et al.* (2015a) presented single grain OSL ages in better agreement with independent age control when calculating Unweighted Arithmetic Means (UAM) of individual equivalent doses, compared to Central Dose Model (CDM)-based ages (Galbraith *et al.*, 1999; following Bailiff *et al.*, 2013, we prefer to use the terminology Central Dose Model, rather than Central Age Model as this model only concerns dose estimation – not age). While the UAM approach has the drawback of ignoring analytical sources of uncertainty, Combès *et al.* (2015) proposed a Bayesian model for the statistical analysis of SAR OSL data (hereafter, this model will be referred to as the BaSar model). Based on a reference dataset, Guérin *et al.* (2015b) showed that this model (BaSar) appears to yield more accurate ages than the CDM. In the present study, we have also calculated the Arithmetic Mean of the CDM (AM-CDM[1]). In all three cases (UAM, BaSar and AM-CDM) the sample-characteristic equivalent dose is estimated by an arithmetic mean of individual equivalent doses (UAM), or by the mean of their distribution (BaSar and AM-CDM).

[1] For a D_e distribution characterised by a CAM dose $D \pm \sigma_D$ and relative overdispersion $OD \pm \sigma_{OD}$, we estimate the AM-CDM dose as $e^{Log(D)+\frac{OD^2}{2}}$. Work is in progress on the development of better Mean Dose Model. In this study, by propagating the errors, we estimate the standard error on the AM-CAM dose by $\left(\frac{\sigma_D}{D} + OD\sigma_{OD}\right) e^{Log(D)+\frac{OD^2}{2}}$. This formula was obtained considering that D and OD are not independent parameters (*i.e.* assuming df = (df/dx) dx + (df/dy) dy, where f is he formula for the AM-CAM dose, x is D and y is OD).

Indeed, in dose rate determination, we measure a rate of energy emitted per unit time and mass. For example, using spectrometry techniques, we determine the concentration in K, U and Th, and then convert these concentrations to dose rates by multiplying the concentrations by the specific activity of each radionuclide and by the average energy emitted per disintegration (Guérin *et al.*, 2011). Using the infinite matrix assumption (Roesch and Attix, 1968; Aitken, 1985), this rate is equal to the rate of energy absorption per time and mass. For the simplicity of the argument, let us assume that we have a sediment made of *n* identical grains of quartz, all having the same mass and age *A*. The determined dose rate corresponds to the total (amount of) energy absorbed per unit time and mass in the sample. As a result, since energy is a cumulative quantity, if one grain receives more than the average dose rate, say a fraction *(1+x)* of the dose rate, then the remaining *(n-1)* grains receive, on average, a fraction *(1-x/(n-1))* of the average dose rate. For example, another grain will receive a fraction *(1-x)* of the average dose rate; and all remaining *(n-2)* grains will receive the average. So if we take for the numerator of the age equation the geometric mean of doses received by the grains, we will get an age estimate equal to the square root of $(1-x^2)$ multiplied by the age *A*, which will be less than or equal to *A*. Conversely, taking for the numerator of the age equation the arithmetic mean of doses to quartz grains, our estimate of *A* will be unbiased. This statement can be generalised: no matter what the distribution of dose rates to individual grains is, the invariant parameter is the amount of energy available for the grains, independently of how the radioactivity is distributed in the sample (see Guérin *et al.*, 2012b; Guérin *et al.*, 2015c). Thus, the aim of any statistical modelling should be the average dose received by the grains, rather than the geometric mean of the distribution of doses to individual grains (distribution which is always unknown and not accessible experimentally; Guérin *et al.*, 2015c). In other words, the CDM appears to be based on a biased dose estimator (at least in cases for which the dispersion in single grain doses is important compared to other sources of dispersion in D_e estimates), in contrast with all three other models discussed here (BaSar, AM-CDM and UAM).

In section 3.1.2 (interpretation of natural D_e distributions), we have tested the different models for age calculation; however, only the CDM and UAM have been used to interpret dose recovery data (section 3.1.1).

It is common practice in luminescence dating to perform dose recovery tests. After laboratory bleaching of the natural signal of a sample, a known dose is delivered and subsequently measured to estimate the accuracy of the measurement procedure (including the SAR protocol, the grain selection and the statistical analysis). Guérin *et al.* (2015b) recently showed, based on a set of known-age samples, that there is no significant correlation between the measured to given dose ratio on the one hand, and the OSL to reference age ratio. Nevertheless, such dose recovery tests may be useful in showing trends in data analysis, and to test the effect of selection criteria on controlled datasets.

2.3. Dose rate measurements

Gamma dose rates were measured *in situ* using Al_2O_3:C dosimeters (Richter *et al.,* 2010) and were presented – and their variability discussed – by Guérin *et al.* (2012a). The radioelement contents of the sediment samples were measured by high-resolution, low background gamma spectrometry and converted to dose rates using the factors from Guérin *et al.* (2011). Compared to the previous study of Guérin *et al.* (2012a), only the size of the grains used for OSL analysis was different. To account for beta attenuation, the factors of Guérin *et al.* (2012b) were used. The only new dose-rate measurements in the present study are ICP-MS and ICP-AES measurements of U and Th (MS) and K (AES) for two sets of samples: the sedimentary quartz extracts from 4 samples on the one hand, and the heated flints on the other hand. These results were used to calculate the internal

dose rates; for the quartz grains, the alpha efficiency (5 mGy/10^3 alpha/cm^2) was taken from Tribolo *et al.* (2001) and average K, U and Th contents from ICP-MS and -AES were used, while self-dose factors for beta dose rates were taken from Guérin *et al.* (2012b). This led to an estimate of the internal dose rate to quartz grains of 0.030 ± 0.005 Gy.ka^{-1}. The dose rate values used for age calculations are shown in Tables 1 and 2. For the heated flints, given the relatively low dispersion in the values from Guérin *et al.* (2012a), the average a-value (0.05 ± 0.02; n=13 – the quoted uncertainty corresponds to the relative standard deviation in individual values) was applied to all samples. Cosmic dose rates were measured by *in situ* gamma spectrometry (Guérin et al., 2012). The average water content measured at the time of sampling (12.5 ± 5.0 %) was considered representative of that during the time of burial; this value is the same as that used by Guérin *et al.* (2012).

3. Results

In this section, we present all the luminescence results from TL and OSL independently from each other. In Section 4, we compare these ages to each other as well as to preliminary IRSL ages from K-feldspar (Frouin, 2014) and subsequently refine our analyses.

3.1. OSL D_e distributions and ages

3.1.1. Dose recovery experiments

Initially, all grains for which the uncertainty on the first test dose signal (the 'natural test dose signal') was less than 20% were selected; for the samples that were heated in the past (Bdx 13394, -396 and -397), 34 % of the grains passed this criterion. Conversely, for the unheated samples for which dose recovery tests were performed, this fraction was only 10 %. We interpret this difference in inherent OSL sensitivity to be caused by thermal sensitisation of the grains in the past. Table S1 shows the effect of two classical rejection criteria (based on recuperation and recycling) on the average measured to given dose ratio, for seven dose recovery experiments. Apart from sample Bdx 13394 that was used for two dose recovery experiments (one with a beta irradiation, and the other one with a gamma irradiation), all the other tested samples (Bdx 13396, -397, -408, -409 and -410) were given a known gamma dose (~76 Gy) with a reference ^{137}Cs source at DTU Nutech. We tested rejecting (i) all grains for which the recycling ratio is not consistent with unity, at two standard deviations (17 % of the grains rejected); (ii) all grains showing a significant recuperation signal (>10 % of the natural signal – 4 % of the grains rejected); and (iii) both of these criteria (18 % of the grains rejected). The relative numbers of rejected grains are similar to those of other OSL studies, *e.g.* in Jacobs *et al.* (2008a) the corresponding numbers are (i) 24 ± 1 % and (ii) 1.8 ± 0.2 % (n = 48 samples). However, we observe no significant changes in the dose recovery ratio or in the dispersion in the equivalent dose distribution (*i.e.* overdispersion), despite a significant reduction in the number of selected grains. Thus, we decided, as did Guérin *et al.* (2015a), not to apply these criteria in the analysis of our samples.

The average measured to given dose (76 Gy) ratio is 0.92 ± 0.03 (n=7) when using the UAM, and 0.89 ± 0.03 (n=7) when calculating the equivalent doses with the CDM. In both cases, the average estimated dose is not consistent with – and seems to systematically underestimate – the given dose. The effect of the D_0 selection criterion on the dose recovery data can be seen in Fig. 2; while the fraction of grains in saturation decreases with increasing x to reach negligible values for x~100 Gy (Fig. 2c), the measured to given dose ratio increases with x until it reaches a plateau for x~80 Gy (Figs. 2a and 2b). These results indicate that the D_0 selection criterion is effective in removing early saturating grains. Moreover, the measured to given dose ratio approaches unity when x is increased and thus seems to indicate an increase in accuracy: for D_0 > 105 Gy, the average

dose recovery ratio using the UAM is 0.99 ± 0.03 (n=7; 0.93 ± 0.03 using the CDM). As a result, we decided to keep all grains for which D_0 >105 Gy – this value is the lowest D_0 value in the plateau of measured to given dose ratios, and above this value no grains are rejected due to saturation. Interestingly, the overdispersion parameter is essentially unaffected and varies from, on average (n=7), 12 to 16 % in the tested range of x values. Furthermore, the OD parameter in these dose recovery experiments for samples heated in the past (12 ± 1 %, n=4) is indistinguishable from that obtained with samples that were unheated (13 ± 1 %, n=3).

Finally, the unweighted arithmetic mean seems to be a more accurate estimator of the central dose of interest, as the measured to given dose ratio is closer to unity compared to CDM-based values. This statement does not depend on the x value used to select grains based on their D_0 values. To conclude this section on dose recovery experiments, our SAR protocol seems suitable to the measurement of our natural samples; the D_0 > 105 Gy selection criterion and calculation of unweighted arithmetic mean seem to be an adequate procedure for the statistical analysis of our single grain OSL measurements.

3.1.2. Natural D_e distributions

The effect of the D_0 selection criterion on natural D_e distributions is shown in Fig. 3. Selecting those grains for which D_0 > 105 Gy effectively removes (almost) all of the grains whose natural signal is in saturation (Fig. 3c). Moreover, above this value the equivalent dose does not seem to vary significantly both for unweighted arithmetic mean (Fig. 3a) and CDM-based (Fig. 3b) equivalent doses (except maybe for unheated samples, for which one cannot exclude that D_0 > 120 Gy might be the onset of a plateau). In the following, we used only this selection criterion (except if explicitly stated otherwise).

Examples of quartz OSL D_e distributions for a heated sample (Bdx 13397) and for an unheated sample (Bdx 13409) are shown in Figs. 4 and 5. In the literature, several types of figures have been used to represent such distributions, among which radial plots (*e.g.*, Galbraith *et al.*, 1999), T_n vs De plots (*e.g.*, Thomsen *et al.*, 2005) or more simply histograms; a disadvantage of the latter being that the uncertainties on individual D_e estimates are not displayed (see Galbraith and Roberts, 2012). In Fig. 4, T_n vs De plots and histograms are presented, while Fig. 5 shows a set of three radial plots for each of the two samples (Bdx 13397 and 13409). The different hypotheses underlying the radial plots, and the merits of each type of representation are discussed below.

OSL ages may be affected by several sources of variability, such as post-depositional mixing and/or insufficient exposure to sunlight prior to sediment deposition and burial ("poor-bleaching", *e.g.* Roberts *et al.*, 1999). In such cases, external sources of dispersion are expected to be significant and one expects a greater overdispersion parameter compared to that of for example dose recovery experiments. In the present study, the combustion features provide samples that were heated in the past; thus, poor bleaching cannot contribute to the extrinsic sources of variability. Furthermore, the spatial integrity of the combustion layers – in some cases stacked over each other with undisturbed, cemented ash layers only a few cm apart (Aldeias *et al.*, 2012) – strongly indicates that the sediment lying below the ash crust cannot have been affected by post-depositional mixing with younger layers. For the three samples from combustion features (Bdx 13394, -396 and -397), the OD ranges from (Table 3) 21 ± 4 % (sample Bdx 13396) to 30 ± 3 % (Bdx 13397) and, on average, is 26 ± 4 % (n=3). Such values fall within commonly reported values for well-bleached samples unaffected by post-depositional processes (see *e.g.* the review by Guérin *et al.*, 2015b). It is difficult here to estimate the amount of overdispersion expected from dose rate variability considerations, as the grain size distributions for these samples are bimodal (*cf*. Fig. S1). Nevertheless, relatively low K contents (~0.5

% on average) associated with rather low total dose rates (~1 Gy.ka^{-1}) are expected to give rise to non-negligible dispersion in dose rates to individual grains. Indeed, low dose rates imply that, despite relatively low K content, beta dose rate from potassium contributes to the total dose rate by a significant amount (Table 2); and the low content in potassium, together with the observation that potassium feldspar grains are present in the sediment samples, indicates that a significant source of dose rates is heterogeneously, at the sub-mm scale, distributed in hotspots (Guérin et al., 2015c). The extrinsic overdispersion values, calculated as the quadratic difference between the OD values for natural and dose recovery distributions, range from ~17 to ~27 %; such values indeed lie towards the higher end of expected dispersion values for well-sorted sand samples (*cf*. Fig. 9a of Guérin *et al.*, 2015c).

For comparison, the OD parameter for the unheated sediment samples is, on average, 31 ± 3 % (n=5). Individual OD values range between 29 ± 4 % and 37 ± 5 %, and all are consistent, within (the admittedly large) uncertainties, with the OD values obtained for the heated samples (on average, 26 ± 4 %). As a result, we have decided to calculate OSL ages using central dose models: the CDM, the Unweighted Arithmetic Mean (UAM), the AM-CDM and finally the Bayesian model BaSar (Combès *et al.*, 2015). In the latter case, it should be noted that the curve fitting of the OSL dose response curves consists of the sum of a saturating exponential (as described in section 2.2) and a linear component with a positive slope. As a result, there is by definition no saturation, so no grains have been rejected from the dataset based on their D_0 values. The other three models have been applied to dose distributions, where individual dose estimates have been derived by fitting a single saturating exponential to the individual dose response curves, and only to those grains for which D_0 > 105 Gy (*cf.* section 3.1.2).

The radial plots presented in Fig. 5 correspond to different hypotheses regarding the individual uncertainty estimates on D_e values. In such graphical representations, the most important axis is the horizontal, uncertainty axis. Thus, the key question comes down to what is included in the uncertainty budget. Here we considered three cases: (i) only the analytical errors, including counting statistics, instrument reproducibility and curve fitting errors, are taken into account (Fig. 5: top graphs); (ii) the intrinsic overdispersion, as determined with a dose recovery test, is added to the analytical uncertainties (Fig. 5: middle graphs; see Reimann *et al.*, 2012; Thomsen *et al.*, 2015), and (iii) the total overdispersion of the natural distributions is added to the analytical uncertainties (Fig. 5: bottom graphs). This third graph shows what the uncertainties on individual D_e estimates become when the CDM is applied to the distributions. These sets of radial plots allow visualising the effect of different hypotheses on the appearance of radial plots, highlight the difficulty to rely on visual interpretation of such plots for the interpretation of data, and clearly show that radial plots may not be taken as a universal, objectively appropriate way to represent OSL data.

All the single grain OSL ages are shown in Table 3 (see also Fig. S2). Regardless of which model is used to calculate OSL ages, the dispersion in ages is small compared to the individual uncertainties, *i.e.* all ages are essentially indistinguishable. There is neither a stratigraphic inversion nor an increase in age with increasing depth, which points to a short – compared to 5-10 ka uncertainties inherent to luminescence dating methods in this time range (5-10 % of the ages; *cf*. Guérin *et al.*, 2013) – sediment accumulation at the end of MIS 5.

But before moving on to the comparison with other luminescence ages, which age model should we use for samples presumed to have been well-bleached in the past? At present, empirical evidence based on samples for which independent age information is available (Thomsen *et al.*, 2016; n=4 samples; Guérin *et al.*, 2015b; n=19– including the 4 previously mentioned) have shown that CDM-based ages tend to provide systematically underestimated OSL ages.

In the present study, to compare the ages obtained with the different central or mean dose models, we have assumed a short sediment deposition history for the whole sequence, *i.e.* we have assumed that all ages date the same event. In other words, we have assumed that the whole dispersion in OSL ages from Layers 2 to 9 comes from our measurement uncertainties; thus, we have calculated an average OSL age for the complete, instantaneous (at the 5-10 ka scale corresponding to individual age uncertainties) sedimentary accumulation at Roc de Marsal. The average age is 81 ± 2 ka (CDM), 86 ± 2 ka (BaSar), 87 ± 2 ka (UAM), or 88 ± 2 (AM-CDM). It should be emphasised that the errors of the means calculated here are only indicators, in the sense that no modelling was performed to correctly disentangle systematic from random sources of uncertainties. Such modelling goes beyond the scope of this work but would be necessary for a proper comparison of ages. Nevertheless, CDM doses are systematically lower than those estimated with all other models (by, on average, ~5 to 7 %; Fig. S2). Moreover, the three other models yield indistinguishable ages. It clearly appears on Fig. 5 (bottom radial plots) that, since the overdispersion is the main source of dispersion in D_e values, all the most precise D_e estimates – on the right of the graphs – end up with approximately the same precision (cf. the edge and cluster of grains on the right of the radial plots) and are thus given the same weight in the central dose calculation using the CDM. To further investigate this point, in Table 3 a column shows the Unweighted Geometric Mean (UWM) of D_e values: the results are indistinguishable from those given by the CDM, and the average UWM/CDM ratio is 0.99 ± 0.01. In other words, the CDM cannot be preferred to the UAM on the grounds that the former includes individual uncertainties, whereas the latter does not; in effect, the CDM provides values indistinguishable from unweighted geometric means.

We thus have an explanation for the systematic CDM age underestimation (based on simple dose rate considerations – *cf.* section 2.2) given that the geometric mean of a distribution is always smaller than or equal to the corresponding arithmetic mean, and three independent models (whose validity, at least for two of them, has been tested against independent age control) giving essentially the same ages, so we decided to dismiss the CDM ages. But how to choose between the remaining three models? The main weakness of the UAM is that it ignores OSL measurement uncertainties; its strength is that it does not fit a specific dose distribution to the experimental data, conversely to the BaSar moel and the AM-CDM. From this perspective, given the commonly asymmetric distributions of dose rates (whenever hotspots, like ubiquitous K-feldspar grains, are present in the sediment – *cf.* Nathan *et al.*, 2003; Brennan, 2006; Mayya *et al.*, 2006; Cunningham *et al.*, 2012; Guérin *et al.*, 2015c), the AM-CDM is probably better adapted to most Quaternary sediments than the BaSar model. Nonetheless, the BaSar ages appear to be more precise (*i.e.*, yield lower uncertainties) than the UAM and the AM-CDM ages: the average statistical uncertainty on central dose is 3 % with the Basar model, compared to respectively 5 and 6 % for the UAM and AM-CDM (see Table 3). Since there is no significant difference between the ages (and since the accuracy of this model is better than that of the CDM), we favour the model giving us the lowest uncertainties, *i.e.* the BaSar model.

3.2. TL ages

Dose rates, equivalent doses (calculated using the signal between 350 and 400°C) and TL ages for the six dated flints are shown in Table 1. All these ages are, within uncertainties, in stratigraphic order. Two ages were obtained from Layer 2 (39 ± 3 ka and 49 ± 4 ka), one from Layer 3 (53 ± 4 ka) and Layer 4 (50 ± 4 ka), and two from Layer 6 (57 ± 4 ka and 46 ± 3 ka). Thus, all the ages obtained most likely indicate occupations, for the higher part of the sequence, during MIS 3.

4. Discussion

4.1. Which chronology for the Roc de Marsal sequence?

As before (Guérin *et al.* 2012a), we are thus facing two alternative chronological scenarios for the sequence (Fig. 6): OSL gives a short and old chronology – all single grain OSL ages are indistinguishable from each other and point to an age of ~86 ka for the whole sequence (Table 3), while TL indicates a more recent, longer period of successive human occupations (from ~65-70 ka for Layer 9 – *cf*. Guérin *et al.*, 2012a – up to ~40 ka for Layer 2). The two scenarios are inconsistent with each other; here, it should be noted that even with the more classical OSL CDM ages, the two chronologies remain statistically very different.

An advantage of luminescence dating methods is that several signals from various minerals can be used for establishing robust chronologies. Frouin (2014) studied the post-IR IRSL at 225 °C (pIR_{225}: Thomsen *et al.*, 2008; Buylaert *et al.*, 2009) of coarse-grain (200-250 µm) K-feldspar extracts from the sediment samples Bdx 13401, -402, -403, -404, -405, -406 and -407. Thus, we have a direct comparison with the OSL of the present study for samples Bdx 13401 and 13402; for the other samples, we can compare these results with the fine grain multi-grain OSL ages of Guérin *et al.* (2012a), and view the ages in their stratigraphic position.

Preliminary K-feldspar pIR_{225} ages (Frouin, 2014) are also shown in Fig. 6 and show excellent agreement with the flint TL ages. These pIR_{225} ages were corrected for fading and for the presence of a hard-to-bleach component; for further details, the reader is referred to Frouin (2014). This agreement is interesting, because the TL and pIR_{225} ages can be considered to be close to independent from each other: the only common factor in these two sets of ages is the sum of gamma and cosmic dose rates, which amounts to, on average, ~57 % of the total dose rate to heated flints but only ~19 % of the total dose rate to feldspar. Thus, the comparison of TL and OSL with pIR ages tends to confirm the conclusions of Guérin *et al.* (2012a) and to indicate that their TL chronology was reliable (in contrast with their apparently over-estimated multi-grain, fine grain OSL ages). From this perspective, the newly obtained TL ages strengthen the previous flint TL chronology from Guérin *et al.* (2012a).

Conversely, quartz OSL ages appear to be systematically older than both flint TL and K-feldspar IRSL ages. How can we explain this pattern, and can we resolve it with appropriate statistical modelling? The single grain OSL ages presented so far were calculated assuming that the OSL signal had been completely reset before burial. However, a common source of overestimation in OSL ages lies in an insufficient exposure of sedimentary grains to sunlight during sediment transport (*e.g.*, Roberts *et al.*, 1999; Thomsen *et al.*, 2007; Medialdea *et al.*, 2014). This being said, it is well-know that the IRSL signals, and in particular the post-IR IRSL signals, reset much slower (more than an order of magnitude) than quartz OSL when sediments are exposed to sunlight (Godfrey-Smith *et al.*, 1988; Buylaert *et al.*, 2011; Murray *et al.*, 2012). So it is actually quite surprising to obtain quartz OSL ages greater than K-feldspar IRSL ages; it indicates that the problem of age discrepancy cannot be due to sediment transport, and thus must be due to other factors having affected the sediment after their transport to the cave. Roc de Marsal is a small, natural cavity part of a karstic system. Frequent roof spall events resulted in the presence of a great amount of limestone in the sediment, but also boulders and gravel fallen from the bedrock. Fig. 7 shows a photomicrograph of a thin section from a block of bedrock; besides limestone, a number of sand- and some silt-sized, quartz grains can be seen. Conversely, feldspar grains are virtually absent in the bedrock. Thus, the erosion of limestone may have resulted in quartz grains falling from the cave roof and walls directly on the sedimentary surface. This led us to formulate the hypothesis that our quartz extracts were contaminated by grains that originated from the bedrock and were deposited in the sediment; such grains would virtually not have been transported and as a result would have seen little sunlight prior to burial.

This contamination would not only explain the unusual age discrepancy between quartz OSL and K-feldspar pIR_{225}, but it could also explain two features of the single grain OSL D_e distributions: on the one hand, the greater OD values of the unheated samples compared to those of the heated samples (the latter ones do not suffer from partial bleaching due to their past heating), especially since this differential OD pattern was not observed in dose recovery distributions; and the greater amount of grains in saturation for the unheated samples, compared to the heated ones (*i.e.* on average 26 % for unheated and 14 % for heated samples, *cf*. Fig. 3c). Here it should be noted that for the dose recovery D_e distributions, the heated samples exhibited less grains in saturation (9 %) than unheated samples (11 % - in both cases, these figures correspond to the fraction of grains in saturation before filtering the grains with respect to their D_0 values), but this difference was small compared to that observed for the natural D_e distributions. In principle, we would expect infinite ages for bedrock samples from Roc de Marsal; in particular, it is surprising that we are able to remove all grains in saturation using the D_0 selection criterion (unless, for some reason, bedrock grains exhibit lower D_0 values than other grains in the sediment). However, similar observations (finite D_e values) with grains from bedrock samples were reported elsewhere in comparable contexts (Contrebandiers Cave: Jacobs *et al.*, 2011), even although the calcareous bedrock may be of Pleistocene age in this case – which could explain the finite D_e values. Thus, the assumption that best fits our observations is that endokarstic processes lead to limited, insufficient exposure of quartz grains from the bedrock at the time of sediment deposition.

As a result, we decided to calculate minimum ages from the single grain OSL data. We used the average OD value for the heated samples (26 ± 4 %, n=3) to run the Minimum Age Model (Galbraith *et al.*, 1999; hereafter referred to as the Minimum Dose Model, or MDM). In this study, we favoured the MDM over the Finite Mixture Model (FMM) as we have no reason to believe that the grains assumed to be derived from roof spall (*i.e.* with higher doses) would form a D_e component with an OD value similar to that of the component of the grains expected to be well-bleached. At present, a better accuracy of the AM-MDM (derived from the MDM like the AM-CDM is derived from the CDM, *i.e.* using the formula given in the footnote, section 2.2, where D is the MDM dose, and OD is the input overdispersion value used to run the MDM) has not been demonstrated in the literature; however, the arithmetic mean of the dose distribution fitted by the MDM (rather than the geometric mean dose, *i.e.* the MDM outcome), from first principles, should also – like the AM-CDM compared to the CDM – be better matched with the arithmetic mean dose rate. The results of the AM-MDM are shown in Table 4; as can be seen, the discrepancy between OSL ages, on the one hand, and TL and IRSL ages on the other, is reduced but there is still a systematic overestimation of OSL ages: the average quartz OSL age for the Quina Mousterian layers is ~71 ka (Layers 2-4) as opposed to 49 ka (average of flint TL ages for the same Layers, n=5, including two samples from these layers published by Guérin *et al.*, 2012) and 47 ka (average of K-feldspar pIR_{225} ages for the same Layers, n=3).

What other factors might explain the overestimated OSL ages? Gamma dose rates do not seem to be a good candidate to explain this given the good agreement between flint TL ages (which depend strongly on gamma dose rates) and pIR_{225} ages (which only weakly depend on gamma dose rates). However, observation of impregnated sediment reveals the abundance of small (mm size) lumps of limestone (they are particularly visible in Fig. 9c of Guérin *et al.*, 2012a). For the determination of beta dose rates by high-resolution, low background gamma spectrometry measurements, the sediment samples were completely crushed before any sieving or specific selection process (Guérin *et al.*, 2012a). However, quartz grains – except for those originating from degraded bedrock – were located not in the limestone fragments but in the sedimentary matrix filling the voids between these lumps. Given that limestone has a very poor concentration of radioelements (*cf*. gamma dose rate of ~0.15 $Gy.ka^{-1}$ measured in the bedrock compared to ~0.5

$Gy.ka^{-1}$ in the stratigraphic sequence, see Figs. 7a and b in Guérin *et al.*, 2012a), its presence causes significant beta dose rates heterogeneities. Thus, it is likely that the average beta dose rate over the whole samples is not representative of the beta dose rate to the dated quartz grains, which are located between the lumps of limestone. An adjusted dose rate model was proposed for similar cases by Jacobs *et al.* (2008b), but among other shortcomings highlighted by Guérin *et al.* (2013), a major problem of this model is that the adjusted dose rate is not estimated independently from D_e values, thus leading to serious problems when assessing uncertainties.

In order to try to estimate a more appropriate dose rate value independently from the measurement of equivalent doses, we estimated the average amount of $CaCO_3$ in crushed sediment samples, using a Scanning Electron Microscope coupled with an Energy Dispersive Spectrum (SEM-EDS) system. We determined an average amount of $CaCO_3$ of ~54% (n=6 samples). From this, we made very crude assumptions to estimate the maximum beta dose rate received by quartz grains not contained in $CaCO_3$ lumps: (i) $CaCO_3$ contains no radioelements, and (ii) the quartz grains are not influenced by $CaCO_3$, *i.e.* in each direction all quartz grains are surrounded by 2 mm of non-calcareous sediment; as a result, we assume that the only effect of $CaCO_3$ is to dilute the radioelements (note: here we work on orders of magnitude, a more thorough analysis should also take into account the specific energy absorption coefficients of limestone, *cf*. Nathan and Mauz, 2008). Based on these assumptions and on the average $CaCO_3$ content, we calculated, for each sample, the radioelement contents in the non-calcareous volumetric fraction and then recalculated crude maximum beta dose rates. In other words, we re-calculated the mass of the sediment samples on which gamma spectrometry was performed, by dividing this mass by 1.54 (mass ratio of non-calcareous + calcareous sediment to non-calcareous sediment), which is equivalent to multiplying the beta dose rate values by 1.54. The corresponding indicative ages are given in Table 4. Because of the crudeness of the model we have not associated uncertainties with these indicative ages. However, the agreement between these indicative OSL ages and the other luminescence ages is very good (Fig. 8): the average OSL indicative age for the samples from Quina Layers (Layers 2 to 4) is 56 ka, while the average age for the three samples from Layer 9 is 67 ka. The assumptions made above thus appear to be plausible; obviously, the obtained ages should not be taken for more than what they really are, *i.e.* merely indicative ages (note that for the sake of consistency, pIR_{225} ages should also be recalculated accordingly; here, our aim is simply to test the assumption that underestimated beta dose rates may be the cause of overestimated OSL ages). Their merit is to show that, with simple, reasonable assumptions we can get three sets of more or less independent ages in agreement with each other. This agreement strongly supports the two chronologies given by TL on heated flints (this study; Guérin *et al.*, 2012a) and pIR_{225} from Frouin (2014). Finally, sieving to eliminate mm-size limestone lumps would certainly have led to more accurate OSL ages in the first place.

4.2. Implications for the Mousterian in southwest France

The flint TL ages for the Quina Mousterian layers from Roc de Marsal cluster around 49 ka (average of n=5 samples; Layers 2 to 4). A recurring question of importance in dating archaeological sites and, at a wider scale, particular Palaeolithic material cultures or techno-complexes, is that of their duration. This quantity can be estimated by distinguishing the spread in ages that is due to the lapse of time between the youngest and oldest dated events, from the dispersion in observed ages arising from measurement uncertainties. At present, contrary to what has been proposed for radiocarbon dating (*e.g.,* OxCal: Bronk Ramsey, 2009), no such tool exist to specifically deal with luminescence ages. In particular, there is no way of properly treating the systematic errors that appear in the age calculations and that, in our case of flint TL dating, mainly affect the determination in K, U and Th contents; so there is no straightforward means of extracting these errors from the

total uncertainties. This being said, even if we deal with the sum of several factors (the alpha and beta dose rates from the different radioelements involved), each being affected by its own systematic, relative error, these systematic errors tend to draw all ages in the same direction, which means that they cannot explain a significant part of the spread in apparent ages. However, they appear in the provided age uncertainties. Another specificity of flint TL age uncertainties is that gamma dose rates are not measured at the sample location, which leads to large random, rather than systematic, errors (since the location of heated flints is unknown before the excavations); as a result, in practice the spread in measured gamma dose rates is (almost) always much larger than analytical uncertainties (both random and systematic – on the latter point, see Richter *et al.*, 2010; Miallier *et al.*, 2009, for the block of bricks used at IRAMAT-CRP2A for calibration), which makes the assessment of gamma dose rate uncertainties a difficult task. We estimated these uncertainties based on the spread in measured gamma dose rates as close as possible to the sample location, but we must recognise that the calculation of these uncertainties is not as straightforward, and thus not as reliable, as *e.g.* those related to counting statistics. As a result, TL ages on flints are not the best candidates for statistical modelling; and at present the available statistical models are not perfectly suited for the task.

Nevertheless, to estimate the amount of dispersion in these ages, on top of analytical uncertainties, we ran the CDM on the 5 flint TL ages from Quina Mousterian layers (Layers 2-4). The OD is 11 ± 5 %, which can be explained in two alternative ways: (i) it may reflect our inability to correctly evaluate the errors on gamma dose rates, due to the inadequacy of sample (flint) and gamma dose rate measurement locations. Increasing the uncertainties on gamma dose rates to flint samples by ~20% would indeed result in null overdispersion in the TL ages; or (ii) it could also be interpreted as a time lapse of 11 ± 5 % of 48 ka (central age value obtained with the CDM), *i.e.* 5.3 ± 2.4 ka between the first and the last Quina Mousterian occupations at Roc de Marsal (to the extent that the selection of dated flints represents the whole duration of occupations). It should be emphasised that this value should be treated with caution, for the previously mentioned reasons but also because the model is applied to only 5 samples.

An age of ~49 ka (simple average) for the Quina Mousterian of Roc de Marsal is consistent with other published ages (*e.g.,* Pech de l'Azé IV, McPherron et al., 2012; Richter et al., 2013b) for this techno-complex (see also Guibert *et al.,* 2008 for an overview of previously published ages, even although most of those cannot be given too much credit because of apparent methodological problems). For instance, TL ages from Combe-Capelle Bas yielded similar results (between 37 ± 3 and 57 ± 4 ka) for assemblages that are low on scrapers but fit within Quina technology (Dibble and Lenoir, 1995; Valladas *et al.,* 2003). However, these ages also overlap with recently dated MTA assemblages (*e.g.*, Soressi *et al.,* 2013; McPherron *et al.,* 2012). When taken together with the recently obtained TL ages (weighted average: 73 ± 8 ka) for the Quina Mousterian at Jonzac (Richter *et al.*, 2013a), the ages for the Quina Mousterian of Roc de Marsal also suggest a long duration for this techno-complex. At the same time, these ages conflict with chronological models recently forwarded based in large part on the fauna. Such models place reindeer dominated Quina assemblages at the end of MIS 4: 59-67 ka (Morin *et al.*, 2014), or 60-63 ka (Heinrich Event 6: Discamps *et al.* 2011; Discamps and Royer, this issue). There are later reindeer dominated assemblages that might be correlated to Heinrich Event 5 and would be consistent with the Roc de Marsal ages, *e.g.* La Quina Level 8 (Higham, 2011; Valladas *et al.*, 1999) or Le Moustier Layers G1-2 (Gravina and Discamps, 2015), even although in the latter case the number of faunal remains is small; Combe-Grenal Level 7 (despite, again, a relatively limited sample size; Guadelli, 1987) could also fit within this pattern, and a dating study in progress should soon provide additional data. Abri Peyrony Level L-3B is reindeer dominated and radiocarbon dated to between 39 and 48 ka cal BP (Soressi *et al.* 2013) and also overlaps with some of the Roc de Marsal ages. However, these assemblages are

not Quina Mousterian. As a result, it seems that our newly obtained ages add variability to the MIS 3 lithic assemblages for the Middle Palaeolithic in southwest France, and contradict the strict succession models of Mellars (1967, 1969, 1996), Jaubert (2011), Discamps *et al.* (2011), Morin *et al.* (2014). To reconcile these issues and refine these statements, a proper chronological modelling of luminescence data, and in particular of the shared errors, would be necessary. In addition, dating more sites, at the regional scale, will be necessary to test these hypotheses.

Finally, our results seem to confirm that Levallois assemblages associated with faunal remains including, in great proportions, forest-adapted species such as red deer and roe deer, but also reindeer, occurred during MIS 4 around 65-70 ka, as suggested by Discamps *et al.* (2011) and Guérin *et al.* (2012a).

5. Conclusion

The comparison between different luminescence dating methods (TL, OSL and IRSL) was implemented with the aim of questioning, and hopefully refining the chronology of the Roc de Marsal sequence as proposed by Guérin *et al.* (2012a). From a geochronology perspective, the agreement of two almost independent methods (TL on heated flints and pIR_{225} on sedimentary K-feldspar extracts) provided key elements to analyse quartz single grain OSL data. This study indeed demonstrates that the analysis of quartz single grain OSL data on its own is a very difficult task, even in a favourable context where some of the samples were both heated in the past and clearly undisturbed after deposition, thus providing a benchmark for the rest of the samples. Two simple hypotheses were necessary to reconcile the quartz single-grain OSL chronology with the flint TL and K-feldspar pIR_{225} datasets (even although the agreement between the three signals remains imperfect, in the sense that the indicative dose rates used for OSL age calculations correspond to an extreme hypothesis), and showed that a significant source of error was dose rate. This demonstrates the complementarity of luminescence dating methods in chronological studies of complex archaeological sites.

Moreover, the present study strengthens the MIS 4 ages for the base of the sequence obtained by Guérin *et al.* (2012a), characterised by Levallois technology and composite faunal spectra (presence of red deer, roe deer, and reindeer). Conversely, the upper Layers 2-4, characterised by Quina Mousterian and with faunal spectra dominated by reindeer, are dated to the MIS 3. Finally, based on our luminescence chronology, at Roc de Marsal the transition between MIS 4 and 3 most likely to correspond to Layers 5 and 6 (*i.e.* either occurred during the deposition of Layer 5, or 6, or just before/after).

Acknowledgements

This work was supported by a H.C. Ørsted postdoctoral grant awarded by The Technical University of Denmark to G.G. The research at Roc de Marsal had the financial support of the US National Science Foundation (Grants #0917739 and #0551927), the Leakey Foundation, the University of Pennsylvania Research Foundation, the Service Régional de l'Archéologie, and the Conseil Général de la Dordogne. The Région Aquitaine is also thanked for financial support through the program entitled "Chronologie, Préhistoire et Paléoenvironnements" and through the CHROQUI program. Support was also provided by the LaScArBs Labex (Project number ANR-10-LABX-52, in particular via the NEMO

program). The authors are grateful to Claire Christophe and two anonymous reviewers for constructive and useful comments on an earlier version of this article.

References

Aitken, M. J., 1985. Thermoluminescence dating. Academic Press, London, 359 p.

Aitken M.J., 1998. An introduction to optical dating. Oxford University press, Oxford, 267 p.

Aldeias, V., Goldberg, P., Sandgathe, D., Berna, F., Dibble, H.L., McPherron, S. P., Turq, A., Rezek, Z., 2012. Evidence for Neandertal use of fire at Roc de Marsal (France), Journal of Archaeological Science, 39, 2414-2423.

Arnold, L.J., Demuro, M., Parés, J.M., Pérez-González, A., Arsuaga, J.L., Bermúdez de Castro, J.M., Carbonell, E. 2014. Evaluating the suitability of extended-range luminescence dating techniques over Early and Middle Pleistocene timescales: published datasets and case studies from Atapuerca, Spain. Quaternary International xxx, 1–24.

Bailiff, I.K., Lewis, S.G., Drinkall, H.C., White, M.J., 2013. Luminescence dating of sediments from a Palaeolithic site associated with a solution feature on the North Downs of Kent, UK. Quaternary Geochronology 18, 135-148.

Bourguignon, L., 1997. Le Moustérien de type Quina : nouvelle définition d'une technique. Thèse de doctorat. Université de Paris X-Nanterre, 2 tomes, 672 pp.

Brennan, B. J. 2006. Variation of the alpha dose rate to grains in heterogeneous sediments. Radiation Measurements 41, 1026-1031.

Bronk Ramsey, C., 2009. Bayesian analysis of radiocarbon dates. Radiocarbon 51, 337–360).

Buylaert J.-P., Murray A.S., Thomsen K.J., Jain M., 2009. Testing the potential of an elevated temperature IRSL signal from K-feldspar. Radiation Measurements 44, 560–565.

Buylaert, J.P., Huot, S., Murray, A.S. & Van den haute, P., 2011. Infrared stimulated luminescence dating of an Eemian (MIS 5e) site in Denmark using K-feldspar. Boreas, 40, 46–56.

Buylaert, J.-P., Jain, M., Murray, A.S., Thomsen, K.J., Thiel, C., Sohbati, R., 2012. A robust feldspar luminescence dating method for Middle and Late Pleistocene sediments. Boreas 41, 435-451.

Bøtter-Jensen, L., Bulur, E., Duller, G.A.T., Murray, A.S., 2000. Advances in luminescence instrument systems. Radiation Measurements 32, 523–528.

Castel, J.-C., Discamps, E., Soulier, M.-C., Sandgathe, D., Dibble, H. L., McPherron, S. P., Goldberg, P., Turq, A., this issue. Neandertal subsistence strategies through a zooarchaeological perspective: The Quina Mousterian at Roc de Marsal (France).

Combès, B., Lanos, P., Philippe, A., Mercier, N., Tribolo, C., Guérin, G., Guibert, P., Lahaye, C., 2015. A Bayesian central equivalent dose model for optically stimulated luminescence dating. Quaternary Geochronology, 28, 62-70.

Cunningham, A. C., DeVries, D. J., Schaart, D. R., 2012. Experimental and computational simulation of beta-dose heterogeneity in sediment. Radiation Measurements, 47, 1060-1067.

Delpech, F., 1996. – L'environnement animal des Moustériens Quina du Périgord. Paléo, 8, 31-46.

Dibble, H. and Lenoir, M., 1995. *The Middle Paleolithic Site of Combe-Capelle Bas (France)*. University Museum Press, University of Pennsylvania. 363 pp.

Discamps, E., Royer, A., this issue. A cross-scale approach to the palaeoenvironmental conditions of Mousterian hunters in southwestern France (MIS 5-3): combining data from large and small mammal communities.

Discamps, E., Jaubert, J. & Bachellerie, F., 2011. Human choices and environmental constraints: deciphering the variability of large game procurement from Mousterian to Aurignacian times (MIS 5-3) in southwestern France. Quaternary Science Reviews, 30, 2755-2775.

Duller, G.A.T., 2003. Distinguishing quartz and feldspar in single grain luminescence measurements. Radiation Measurements 37, 161-165.

Duller, G.A.T., Bøtter-Jensen, L., Murray, A.S., Truscott, A.J., 1999. Single grain laser luminescence (SGLL) measurements using a novel automated reader. Nuclear Instruments and Methods B 155, 506–514.

Durcan, J.A., Duller, G.A.T., 2011. The fast ratio: A rapid measure for testing the dominance of the fast component in the initial OSL signal from quartz. Radiation Measurements 46, 1065-1072.

Frouin, 2014. Les feldspaths comme support pour la datation par luminescence de gisements archéologiques et de séquences quaternaires d'Aquitaine. PhD thesis, University Bordeaux Montaigne.

Galbraith, R.F., Roberts, R.G., 2012. Statistical aspects of equivalent dose and error calculation and display in OSL dating: an overview and some recommendations. Quaternary Geochronology 11, 1-27.

Galbraith R.F., Roberts R.G., Laslett G.M., Yoshida H., Olley J.M., 1999. Optical dating of single and multiple grains of quartz from Jinmium rock shelter, northern Australia: Part I, experimental design and statistical models. Archaeometry 41, 339–364.

Geach, M.R., Thomsen, K.J., Buylaert, J.-P., Murray, A.S., Mather, A.E., Telfer, M.W., Stokes, M., 2015. Single-grain and multi-grain OSL dating of river terrace sediments in the Tabernas Basin, SE Spain. Quaternary Geochronology 30, 213-218.

Godfrey-Smith, D.L., Huntley, D.J., Chen, W.H., 1988. Optically dating studies of quartz and feldspar sediment extracts. Quaternary Science Reviews 7, 373-380.

Gravina, B., Discamps, E., 2015. MTA-B or not to be? Recycled bifaces and shifting hunting strategies at Le Moustier and their implication for the late Middle Palaeolithic in southwestern France. Journal of Human Evolution 84, 83-98.

Guadelli, J.-L., 1987. Contribution à l'étude des zoocénoses préhistoriques en Aquitaine (Würm ancien et interstade würmien). Thèse de doctorat, Université Bordeaux 1.

Guérin, G., Mercier, N. and Adamiec, G, 2011. Dose-rate conversion factors: update. Ancient TL 29, 5-8.

Guérin, G., Discamps, E., Lahaye, C., Mercier, N., Guibert, P., Turq, A., Dibble, H., McPherron, S., Sandgathe, D., Goldberg, P., Jain, M., Thomsen, K., Patou-Mathis, M., Castel, J.-C., Soulier, M.-C., 2012a. Multi-method (TL and OSL), multi-material (quartz and flint) dating of the Mousterian site of the Roc de Marsal (Dordogne, France): correlating Neanderthals occupations with the climatic variability of MIS 5-3. Journal of Archaeological Science, 39, 3071-3084.

Guérin, G., Mercier, N., Nathan R., Adamiec, G., Lefrais, Y., 2012b. On the use of the infinite matrix assumption and associated concepts: a critical review. Radiation Measurements, 47, 778-785.

Guérin, G., Murray A. S., Jain M., Thomsen K. J., Mercier, N., 2013. How confident are we in the chronology of the transition between Howieson's Poort and Still Bay? Journal of Human Evolution, 64, 314-317.

Guérin, G., Frouin, M., Talamo, S., Aldeias, V., Bruxelles, L., Chiotti, L., Dibble, H. L., Goldberg, P., Hublin, J.-J., Jain, M., Lahaye, C., Madelaine, S., Maureille, B, McPherron, S. P., Mercier, N., Murray, A. S., Sandgathe, D., Steele, T. E., Thomsen, K. J., Turq, A., 2015a. A Multi-method Luminescence Dating of the Palaeolithic Sequence of La Ferrassie Based on New Excavations Adjacent to the La Ferrassie 1 and 2 Skeletons, au Journal of Archaeological Science 58, 147-166.

Guérin, G., B. Combès, C. Tribolo, C. Lahaye, N. Mercier, P. Guibert, K. J. Thomsen, 2015b. Testing the accuracy of a single grain OSL Bayesian central dose model with known-age samples. Radiation Measurements 81, 62-70.

Guérin, G., Jain M., Thomsen K. J., Murray A. S., Mercier, N., 2015c. Modelling dose rate to single grains of quartz in well-sorted sand samples: the dispersion arising from the presence of potassium feldspars and implications for single grain OSL dating. Quaternary Geochronology 27, 52-65.

Guibert, P., Bechtel, F., Bourguignon, L., Brenet, M.,Couchoud, I., Delagnes, A.,Delpech, F., Detrain, L., Duttine, M., Folgado, M., Jaubert, J., Lahaye, C., Lenoir, M., Maureille, B., Texier, J.-P., Turq, A.,Vieillevigne, E., Villeneuve, G., 2008. Une base de données pour la chronologie du Paléolithique moyen dans le Sud-Ouest de la France. Mémoire XLVII de le Société Préhistorique Française, 19-40.

Hansen, V., Murray, A.S., Buylaert, J.-P., Yeo, E.-Y., Thomsen, K.J., 2015. A new irradiated quartz for beta source calibration. Radiation Measurements 81, 123-127.

Higham, T.F.G, 2011. European Middle and Upper Palaeolithic radiocarbon dates are often older than they look: problems with previous dates and some remedies. Antiquity, 85, 235–249.

Hiscock, P., Turq, A., Faivre, J.-Ph., Bourguignon, L., 2009. Quina procurement and tool production. In: Blades, B., Adams, B. (Eds.), Lithic Materials and Paleolithic Societies. Blackwell Edition, pp. 232-246.

Jacobs, Z., Duller, G.A.T., Wintle, A.G., 2006. Interpretation of single grain D_e distributions and calculation of D_e. Radiation Measurements, 41, 264-277.

Jacobs, Z., Roberts, R.G., Galbraith, R.F., Deacon, H.J., Grün, R., Mackay, A., Mitchell, P., Vogelsang, R., Wadley, L., 2008a. Ages for the Middle Stone Age of southern Africa: implications for human behavior and dispersal. Science 322, 733-735.

Jacobs, Z., Wintle, A.G., Roberts, R.G., Duller, G.A.T., 2008b. Equivalent dose distributions from single grains of quartz at Sibudu, South Africa: context, causes and consequences for optical dating of archaeological deposits. Journal of Archaeological Science 35, 1808-1820.

Jacobs, Z., Meyer, M.C., Roberts, R.G., Aldeais, V., Dibble, H., El Hajraoui, M.A., 2011. Single-grain OSL dating at La Grotte des Contrebandiers ('Smugglers' Cave'), Morocco: improved age constraints for the Middle Paleolithic levels. Journal of Archaeological Science 38, 3631-3643.

Jaubert, J., 2011. Les archéo-séquences du Paléolithique moyen du Sud-Ouest de la France: Quel bilan un quart de siècle après François Bordes? In: Delpech, F., Jaubert, J. (Eds.), François Bordes et la préhistoire: Colloque international François Bordes, Bordeaux, 22–24 avril 2009. Éditions du Comité des Travaux Historiques et Scientifiques, Paris, pp. 235–253.

Kristensen, J.A., Thomsen, K.J., Murray, A.S., Buylaert, J.P., Jain, M., Breuning-Madsen, H., 2015. Quantification of termite bioturbation in a savannah ecosystem: application of OSL dating. Quaternary Geochronology 30, 334-341.

Lapp, T., Jain, M., Thomsen, K. J., Murray, A. S. & Buylaert, J. P., 2012. New luminescence measurement facilities in retrospective dosimetry. Radiation Measurements 47, 803–808.

Madsen, A.T., Duller, G.A.T., Donnelly, J.P., Roberts, H.M., Wintle, A.G., 2009. A chronology of hurricane landfalls at Little Sippewisset Marsh, Massachusetts, USA, using optical dating. Geomorphology 109, 36-45.

Mayya, Y.S., Morthekai, P., Murari, M.K., Singhvi, A.K., 2006. Towards quantifying beta microdosimetric effects in single-grain quartz dose distribution. Radiation Measurements, 41, 1032-1039.

McPherron, S.P., Talamo, S., Goldberg, P., Niven, L., Sandgathe, D., Richards, M.P., Richter, D., Turq, A., Dibble, H.L., 2012. Radiocarbon dates for the late Middle Palaeolithic at Pech de l'Azé IV, France. Journal of Archaeological Science 39, 3436–3442.

Medialdea, A., Thomsen, K.J., Murray, A.S., Benito, G, 2014. Reliability of equivalent-dose determination and age-models in the OSL dating of historical and modern palaeoflood sediments. Quaternary Geochronology 22, 11-24.

Mellars, P., 1967. The Mousterian Succession in South-west France. PhD Dissertation. University of Cambridge.

Mellars, P., 1969. The chronology of Mousterian industries in the Périgord region of South-West France. Proceedings of the Prehistoric Society 35, 134–171.

Mellars, P., 1996. The Neanderthal Legacy: An Archaeological Perspective from Western Europe. Princeton University Press, Princeton.

Mellars, P., Grün, R., 1991. A comparison of the electron spin resonance and thermoluminescence dating methods: the results of ESR dating at Le Moustier (France). Cambridge Archaeological Journal 1, 269–276.

Mercier, N., Valladas, H., Valladas, G., 1992. Some observations on palaeodose determination in burnt flints. Ancient TL 10, 28–32.

Miallier, D., Guérin, G., Mercier, N., Pilleyre, T. and Sanzelle, S., 2009. The Clermont radiometric reference rocks: a convenient tool for dosimetric purposes. Ancient TL, 27, 37-44.

Morin, E., Delagnes, A., Armand, D., Castel, J.-C. and Hodgkins, J., 2014. Millennial-scale change in archaeofaunas and their implications for Mousterian lithic variability in southwest France. Journal of Anthropological Archaeology 36, 158-180.

Murray, A. S., Wintle, A. G., 2000. Luminescence dating of quartz using an improved single-aliquot regenerative-dose protocol. Radiation Measurements 32, 57-73.

Murray, A.S., Olley, J.M., 2002. Precision and Accuracy in the Optically Stimulated Luminescence Dating of Sedimentary Quartz: A Status Review. Geochronometria 21, 1-16.

Murray, A. S., Wintle, A. G., 2003. The single aliquot regenerative dose protocol: potential for improvements in reliability. Radiation Measurements 37**,** 377-381.

Murray, A.S., Thomsen, K.J., Masuda, N., Buylaert, J.P., Jain, M., 2012. Identifying well-bleached quartz using the different bleaching rates of quartz and feldspar luminescence signals. Radiation Measurements 47, 688-695.

Nathan R.P, Mauz B., 2008. On the dose-rate estimate of carbonate-rich sediments for trapped charge dating. Radiation Measurements 43, 14-25.

Nathan, R.P., Thomas, P.J., Jain, M., Murray, A.S., Rhodes, E.J., 2003. Environmental dose rate heterogeneity of beta radiation and its implications for luminescence dating: Monte Carlo modelling and experimental validation. Radiation Measurements 37, 305-313.

Richter, D., Dombrowski, H., Neumaier, S., Guibert, P., Zink, A., 2010. Environmental gamma dosimetry for in-situ sediment measurements by OSL of a-Al2O3:C. Radiation Protection Dosimetry 141, 27-35.

Richter, D., Hublin, J.-J., Jaubert, J., McPherron, S.P., Soressi, M., Texier, J.-P., 2013a. Thermoluminescence dates for the Middle Palaeolithic site of Chez-Pinaud Jonzac (France). Journal of Archaeological Science 40, 1176-1185.

Richter, D., Dibble, H., Goldberg, P., McPherron, S.P., Niven, L., Sandgathe, D., Talamo, S., Turq, A., 2013b. The Late Middle Palaeolithic in Southwest France: new TL data for the sequence of Pech de l'Azé IV. Quaternary International, 294, 160-167.

Rittenour, T.M., 2008. Luminescence dating of fluvial deposits: applications to geomorphic, palaeoseismic and archaeological research. Boreas, 37, 613-635.

Roberts R.G., Galbraith R.F., Olley J.M., Yoshida H., Laslett G.M., 1999. Optical dating of single and multiple grains of quartz from Jinmium rock shelter, northern Australia, Part II: results and implications. Archaeometry 41, 365–395.

Roesch W. C. and Attix F. H., 1968. Basic concepts of dosimetry. Radiation dosimetry, Volume I: Fundamentals. F. H. Attix and W. C. Roesch. New York and London, Academic Press.

Sanchez Goñi, M.F., Landais, A., Fletcher, W.J., Naughton, F., Desprat, S., Duprat, J., 2008. Contrasting impacts of Dansgaard–Oeschger events over a western European latitudinal transect modulated by orbital parameters. Quaternary Science Reviews 27, 1136–1151.

Sandgathe, D.M., H.L. Dibble, P. Goldberg, S.P. McPherron, A. Turq, L. Niven, J. Hodgkins, 2011. On the Role of Fire in Neandertal Adaptations in Western Europe: Evidence from Pech de l'Azé IV and Roc de Marsal, France. PaleoAnthropology 2011: 216-242.

Sim, A. K., Thomsen, K. J., Murray, A. S., Jacobsen, G., Drysdale, R.,Erskine, W., 2014. Dating recent floodplain sediments in the Hawkesbury-Nepean River system, eastern Australia using single-grain quartz OSL. Boreas, 43, 1–21.

Soressi, M., McPherron, S.P., Lenoir, M., Dogandzic, T., Goldberg, P., Jacobs, Z., Maigrot, Y., Martisius, N.L., Miller, C.E., Rendu, W., Richards, M., Skinner, M.M., Steele, T.E., Talamo, S., Texier, J.-P., 2013. Neandertals made the first specialized bone tools in Europe. Proceedings of the National Academy of Science 110, 14186–14190.

Thomsen, K.J., Jain, M., Bøtter-Jensen, L., Murray, A.S., Jungner, H., 2003. Variation with depth of dose distributions in single grains of quartz extracted from an irradiated concrete block. Radiation Measurements 37, 315-321.

Thomsen, K.J., Murray, A.S., Bøtter-Jensen, L., Kinahan, J., 2007. Determination of burial dose in incompletely bleached fluvial samples using single grains of quartz. Radiation Measurements 42 (3), 370-379.

Thomsen K.J., Murray A.S., Jain M., Bøtter-Jensen L., 2008. Laboratory fading rates of various luminescence signals from feldspar-rich sediment extracts. Radiation Measurements 43, 1474–1486.

Thomsen K. J., Murray A. S., Jain M., 2012. The dose dependency of the over-dispersion of quartz OSL single grain dose distributions. Radiation Measurements 47, 732-739.

Thomsen, K.J., Kook, M., Murray, A.S, Jain, M., Lapp, T., 2015. Single-grain results from an EMCCD-based imaging system. Radiation Measurements 81, 185-191.

Thomsen, K.J., Murray, A.S., Buylaert, J.-P., Jain, M., Helt-Hansen, J., Aubry, T., 2016. Testing single-grain quartz OSL methods using known age samples from the Bordes-Fitte rockshelter (Roches d'Abilly site, Central France). Quaternary Geochronology 31, 77-96.

Tribolo, C., Mercier, N., Valladas, H., 2001. Alpha sensitivity determination in quartzite using an OSL single aliquot procedure. Ancient TL 19, 47–50.

Turq, A., 1992. Raw material and technological studies of the Quina Mousterian. In: Dibble, H.-L., Mellars, P.A. (Eds.), The Middle Palaeolithic: Adaptation, Behavior, and Variability. University of Pennsylvania, University Museum Monographs n°72, Philadelphia, pp. 75-85.

Valladas, H., Geneste, J.-M., Joron, J.-L., Chadelle, J.-P., 1986. Thermoluminescence dating of Le Moustier (Dordogne, France). Nature 322, 452–454.

Valladas, H., Mercier, N., Falguères, C., Bahain, J.-J., 1999. Contribution des méthodes nucléaires à la chronologie des cultures paléolithiques entre 300 000 et 35 000 ans BP. Gallia Préhistoire, 41, 153-166.

Valladas, H., Mercier, N., Joron, J.L., McPherron, S.P., Dibble, H.L., Lenoir, M., 2003. TL dates for the Middle Paleolithic site of Combe-Capelle Bas, France. Journal of Archaeological Science 30, 1443-1450.

Wintle, A.G., Murray, A.S., 2006. A review of quartz optical stimulated luminescence characteristics and their relevance in single-aliquot regeneration dating protocols. Radiation Measurements, 41, 369-391.

Yoshida, H., Roberts, R. G., Olley, J. M., Laslett, G. M., Galbraith, R. F., 2000. Extending the age range of optical dating using single ‘supergrains’ of quartz. Radiation Measurements, 32, 439-446.

Zhao, Q.Y., Thomsen, K.J., Murray, A.S., Wei, M.J., Pan, B.L., Zhou, R., Zhao, X.H., Chen, H.Y., 2015. Quartz single-grain OSL dating of debris flow deposits from Miyun, north east Beijing in China. Quaternary Geochronology 30, 320-327.

Figure captions.

Fig. 1. (a) Typical TL glow curves (black circles: natural signal; all other symbols represent natural aliquots irradiated in the laboratory with increasing doses – *cf.* legend) and (b) dose response curves for typical flint samples from Roc de Marsal (the data correspond to sample Bdx 16773). For each aliquot, the intensity of the TL signal was normalised by the response to a fixed test dose (38 Gy). A second order polynomial curve was fitted to the data, yielding good results in the investigated dose range. The slide method (Mercier *et al.*, 1992) was used to calculate the equivalent dose.

Fig. 2. Effect of the D_0 selection criterion on dose recovery D_e estimates. The measured to given dose ratio increases when the minimum acceptable D_0 value increases, until a plateau is reached. The mean dose is calculated either with the UAM (a) or with the CDM (b; see text for details). The fraction of grains in saturation decreases with D_0, until it reaches 0 (c). The black squares indicate the average for all tested samples (n=7), while the results for individual samples appear as grey squares.

Fig. 3. Effect of the D_0 selection criterion on natural D_e distributions. The mean (normalised) dose increases when the minimum acceptable D_0 value increases, until a plateau is reached. The mean dose is calculated either with the UAM (a) or with the CDM (b; see text for details). The fraction of grains in saturation decreases with increasing minimum acceptable D_0 values, until it reaches 0 (c). The black squares indicate the average for the unheated sediment samples (n=5), while the red squares indicate the average for the heated samples (n=3). The smaller squares in lighter colours indicate the values for individual samples. Heated samples have less grains in dose saturation, and a less marked effect of the D_0 selection criterion (see the text for interpretation of this behaviour).

Fig. 4. Natural D_e distributions for a heated sample (Bdx 13397, left) and an unheated sample (Bdx 13409, right): the data are displayed both as simple frequency histograms (top) and as scatter plots where the response to the test dose in the first SAR cycle (here called 'Natural test dose response') is plotted as a function of equivalent dose (bottom).

Fig. 5. Radial plots of the natural D_e distributions for two samples: Bdx 13397 (heated sample, left) and Bdx 13409 (unheated sample, right). Top: only the analytical unertainties appear on the horizontal axis; middle: the intrinsic overdispersion (estimated by gamma dose recovery tests) is quadratically added to the analytical uncertainties of each individual D_e estimate; bottom: the natural overdispersion is quadratically added to the analytical uncertainties of each individual D_e estimate. In the latter case, notice the 'edge' on which the most precise grains are clustered on the right of the plots: all the most precise grains are given essentially the same weight by the Central Dose Model (see also Table 3).

Fig. 6. Single Grain OSL ages (calculated assuming that all samples were well-bleached; blue triangles), preliminary pIR_{225} ages (green diamonds; Frouin, 2014) and TL ages: previously obtained on flints (black squares) and heated quartz (purple squares; both datasets Guérin *et al.*, 2012), and from the present study on flints (red squares).

Fig. 7. Photomicrograph of limestone bedrock, showing silt and sand-sized grains of quartz and the virtual absence of feldspar grains; cross-polarised light (XPL).

Fig. 8. TL ages, Single Grain OSL ages calculated assuming (i) partial bleaching due to contamination by quartz from the bedrock, and (ii) overestimated dose rates (see text for details), and preliminary pIR_{225} ages (Frouin, 2014). See the caption of Fig. 6 for details.

Figure 1a

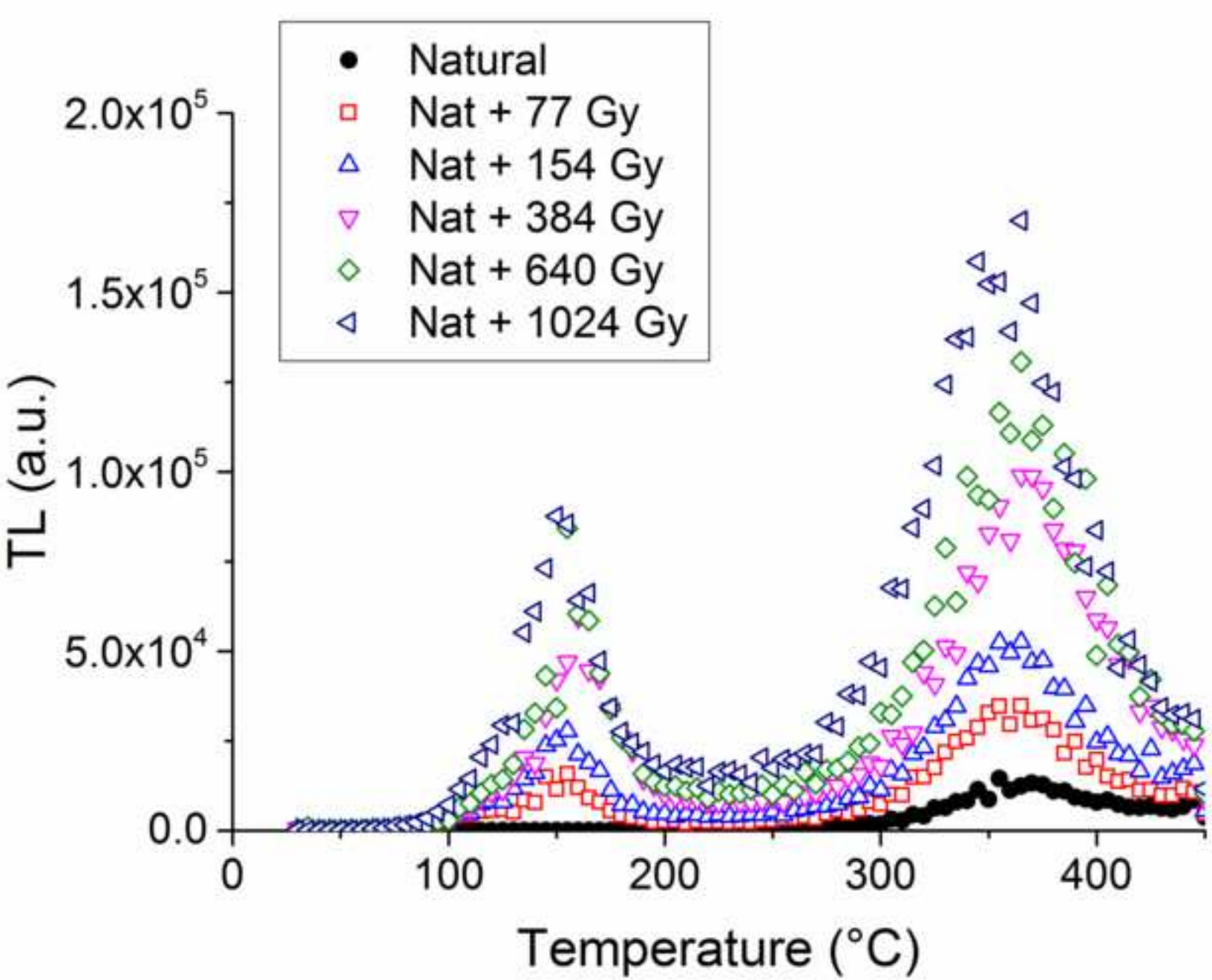
Natural
Nat + 77 Gy
Nat + 154 Gy
Nat + 384 Gy
Nat + 640 Gy
Nat + 1024 Gy
TL (a.u.)
2.0x10^5
1.5x10^5
1.0x10^5
5.0x10^4
0.0
0
100
200
300
400
Temperature (°C)

Figure 1b

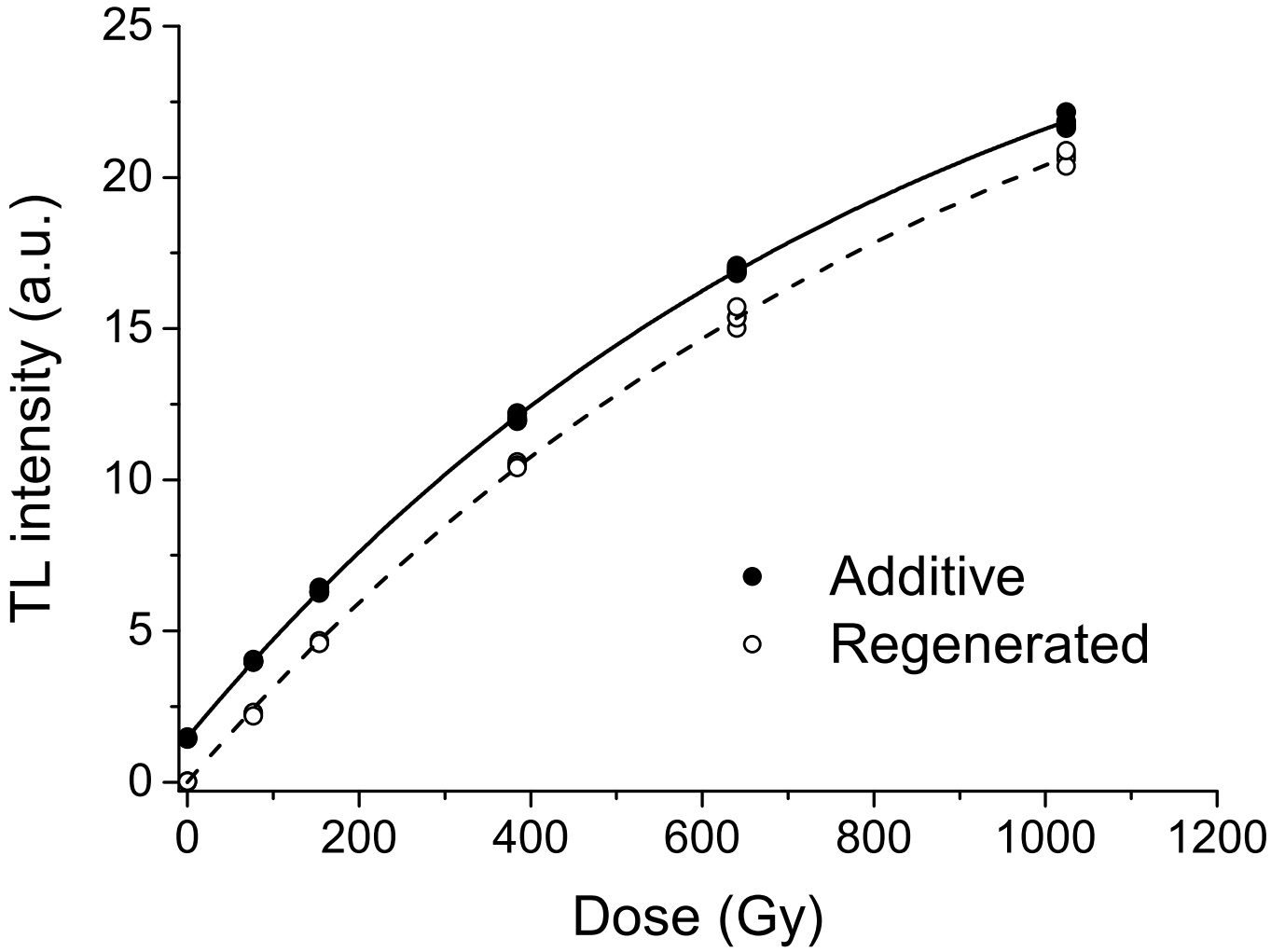
TL intensity (a.u.)
25
20
15
10
5
0
0
200
400
600
800
1000
1200
Dose (Gy)
Additive
Regenerated

Figure 2a

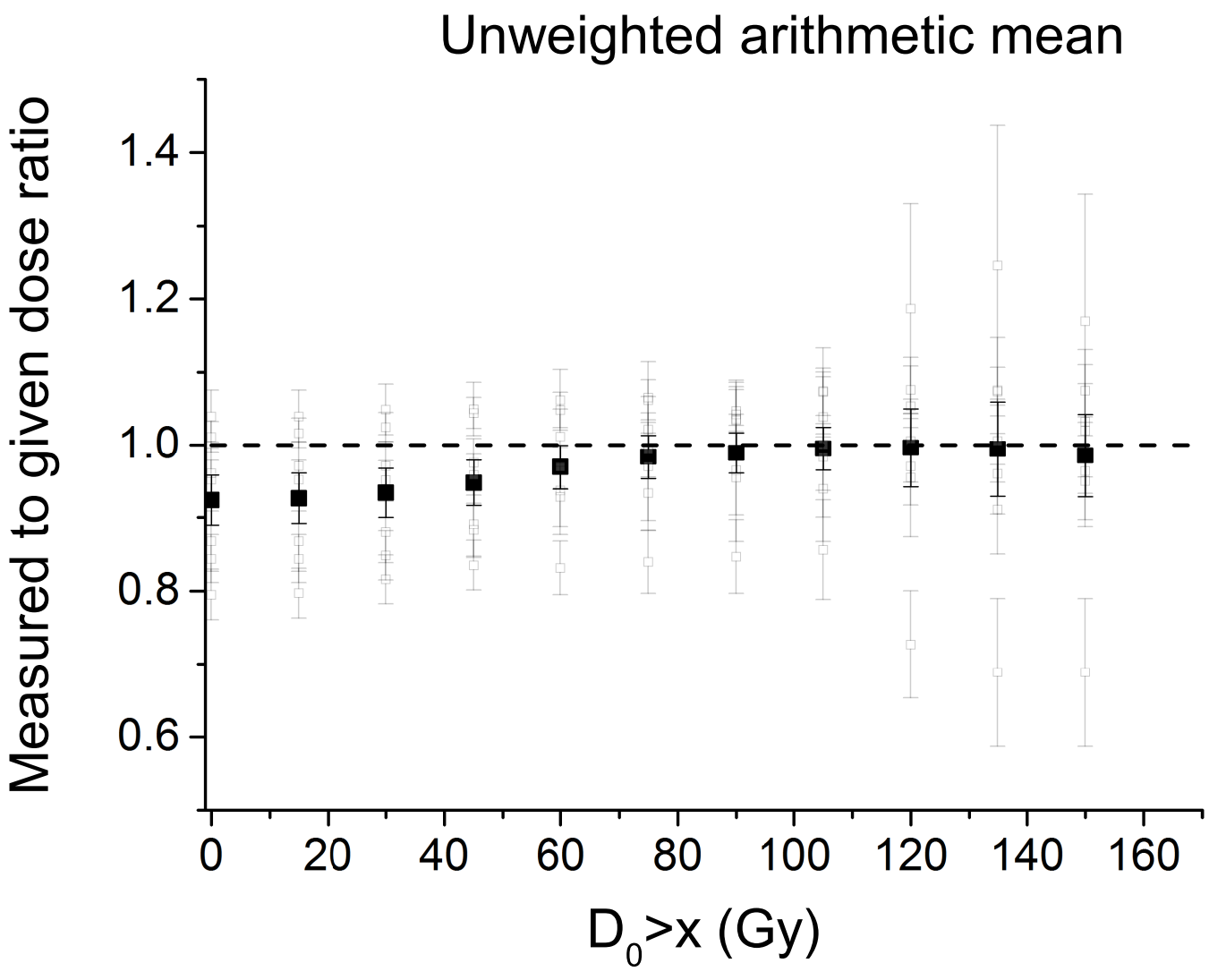
Unweighted arithmetic mean
Measured to given dose ratio
1.4
1.2
1.0
0.8
0.6
0
20
40
60
80
100
120
140
160
D0>x (Gy)

Figure 2b

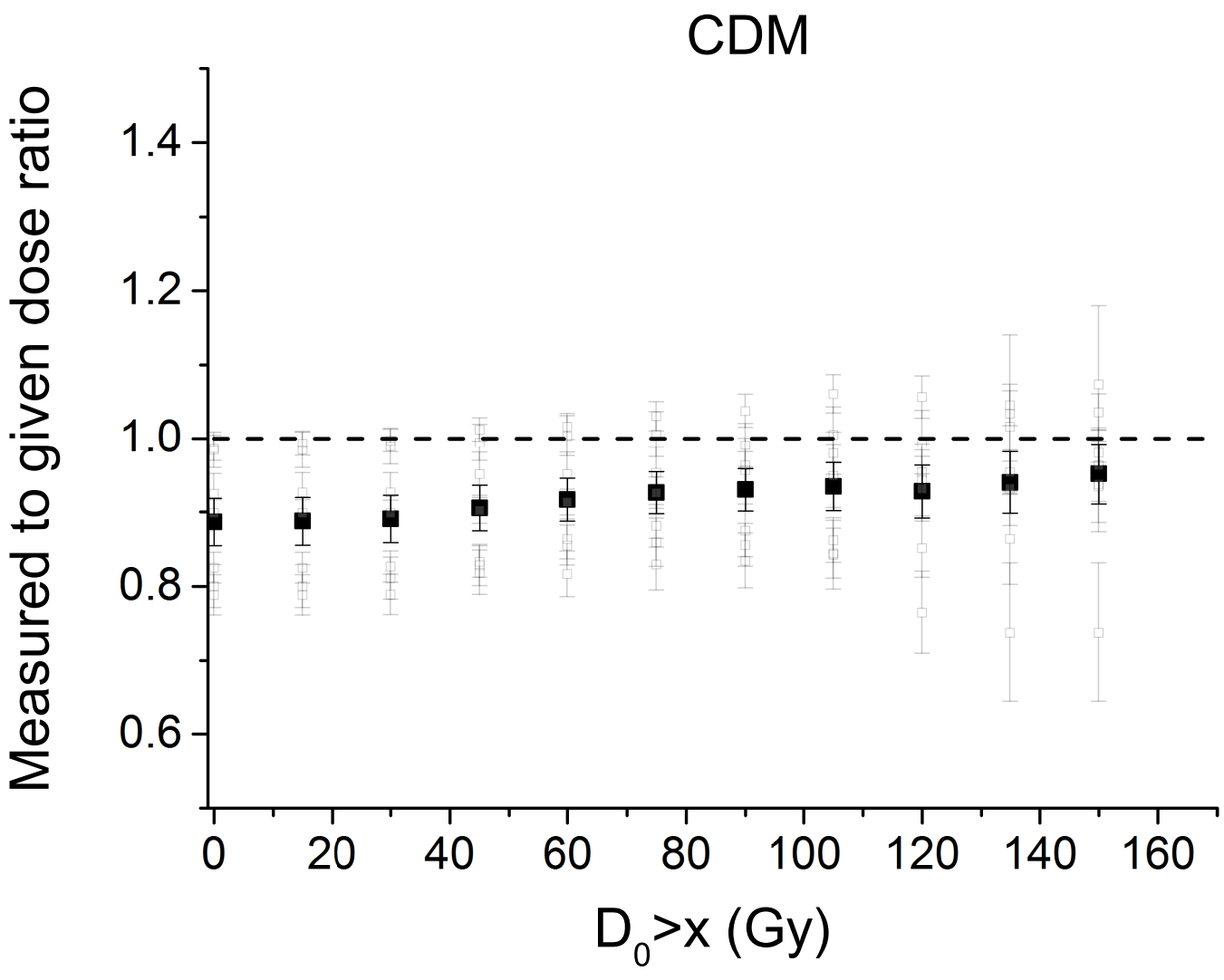
CDM
Measured to given dose ratio
1.4
1.2
1.0
0.8
0.6
0
20
40
60
80
100
120
140
160
D0>x (Gy)

Figure 3b

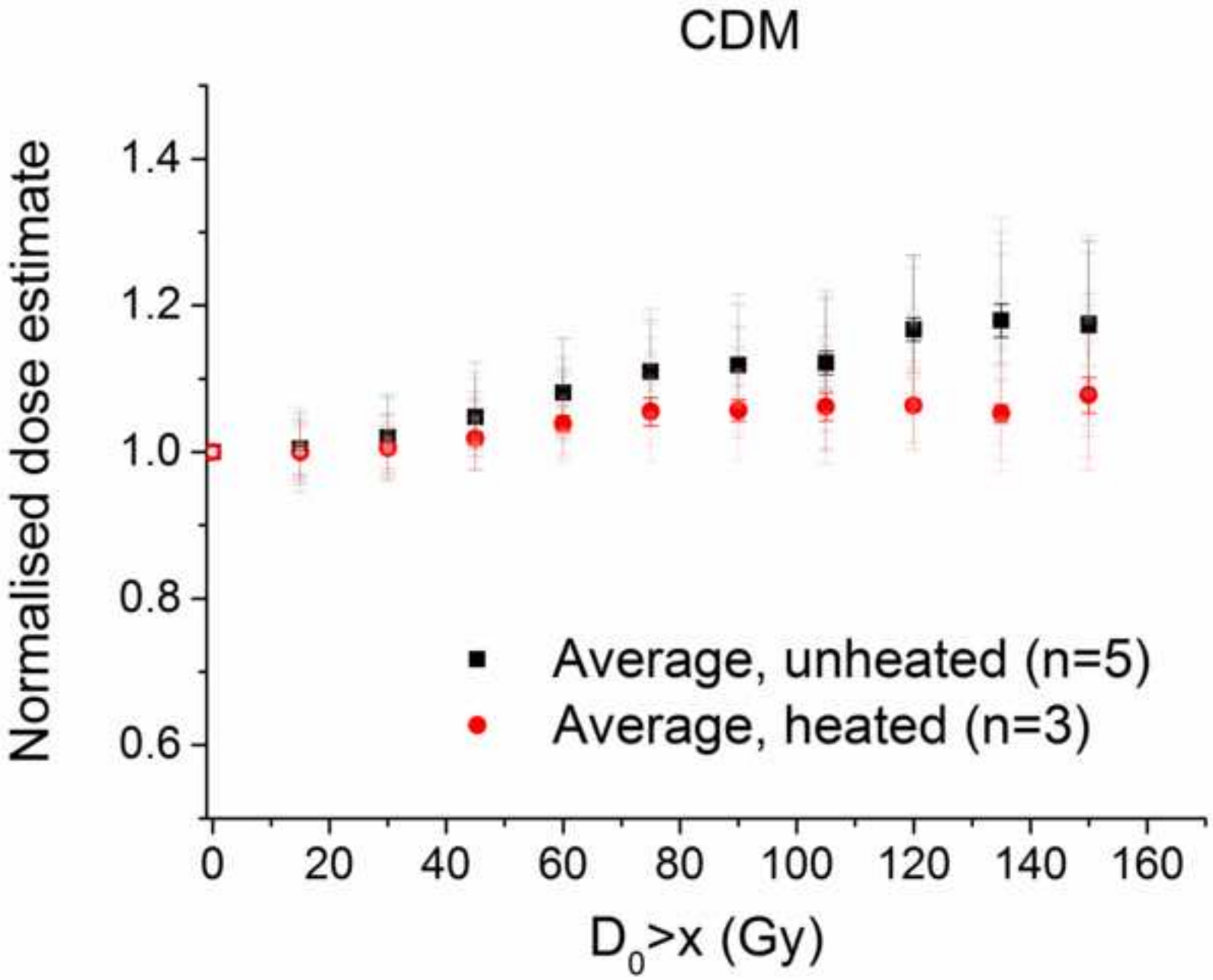
CDM
Normalised dose estimate
1.4
1.2
1.0
0.8
0.6
0
20
40
60
80
100
120
140
160
D0>x (Gy)
Average, unheated (n=5)
Average, heated (n=3)

Figure 4 - TopLeft

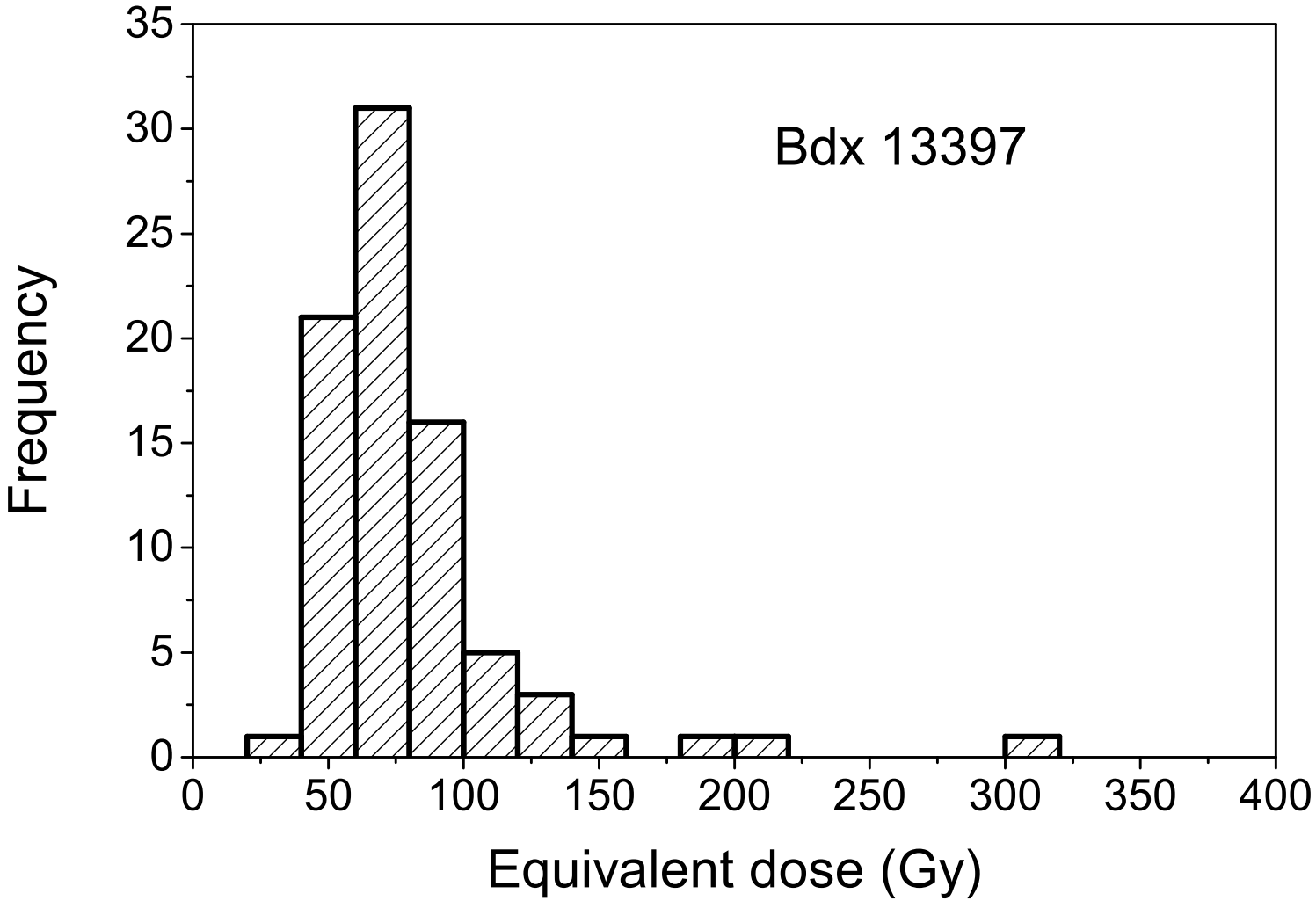

Figure 4 - TopRight

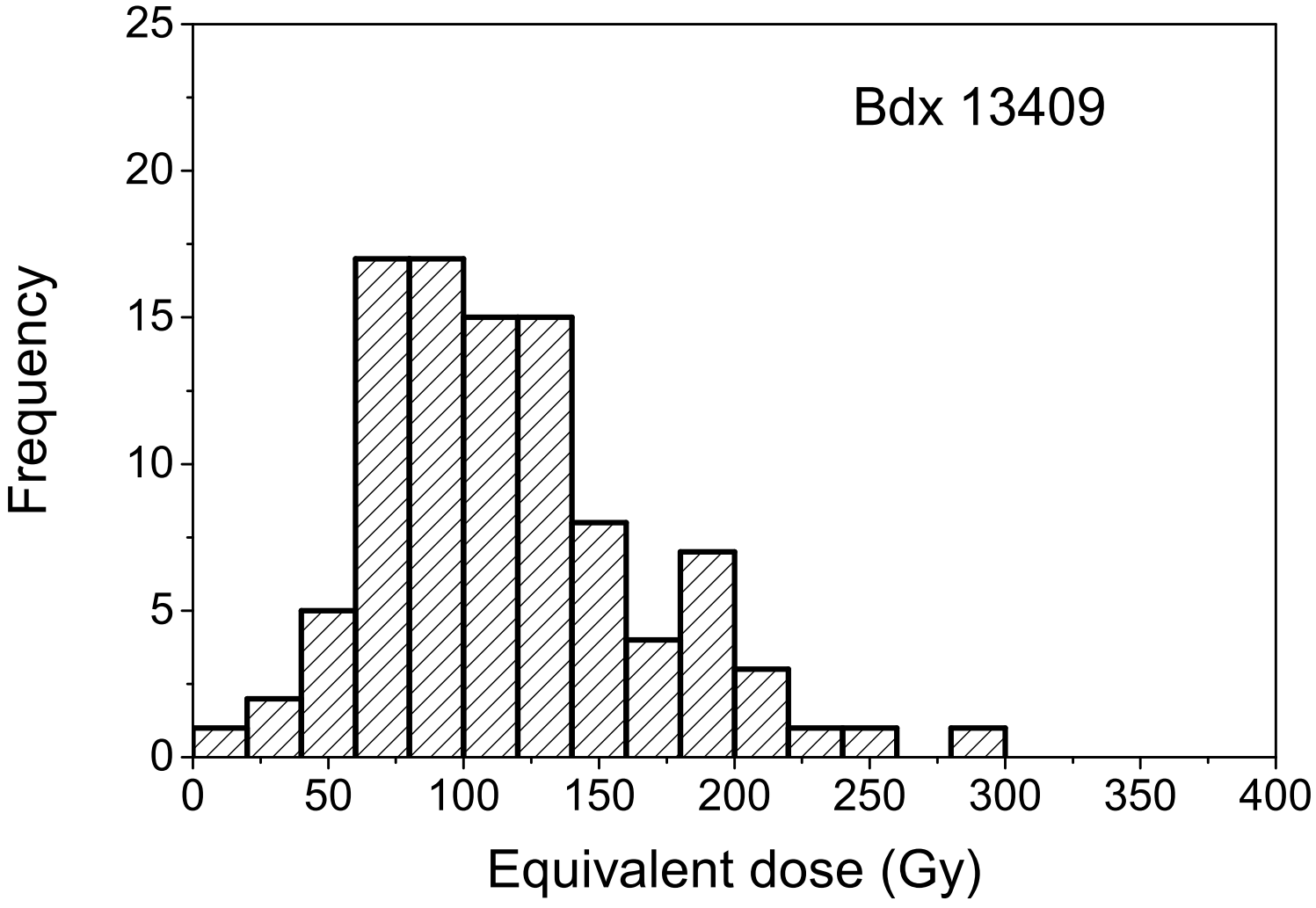

Figure 4 - BottomLeft

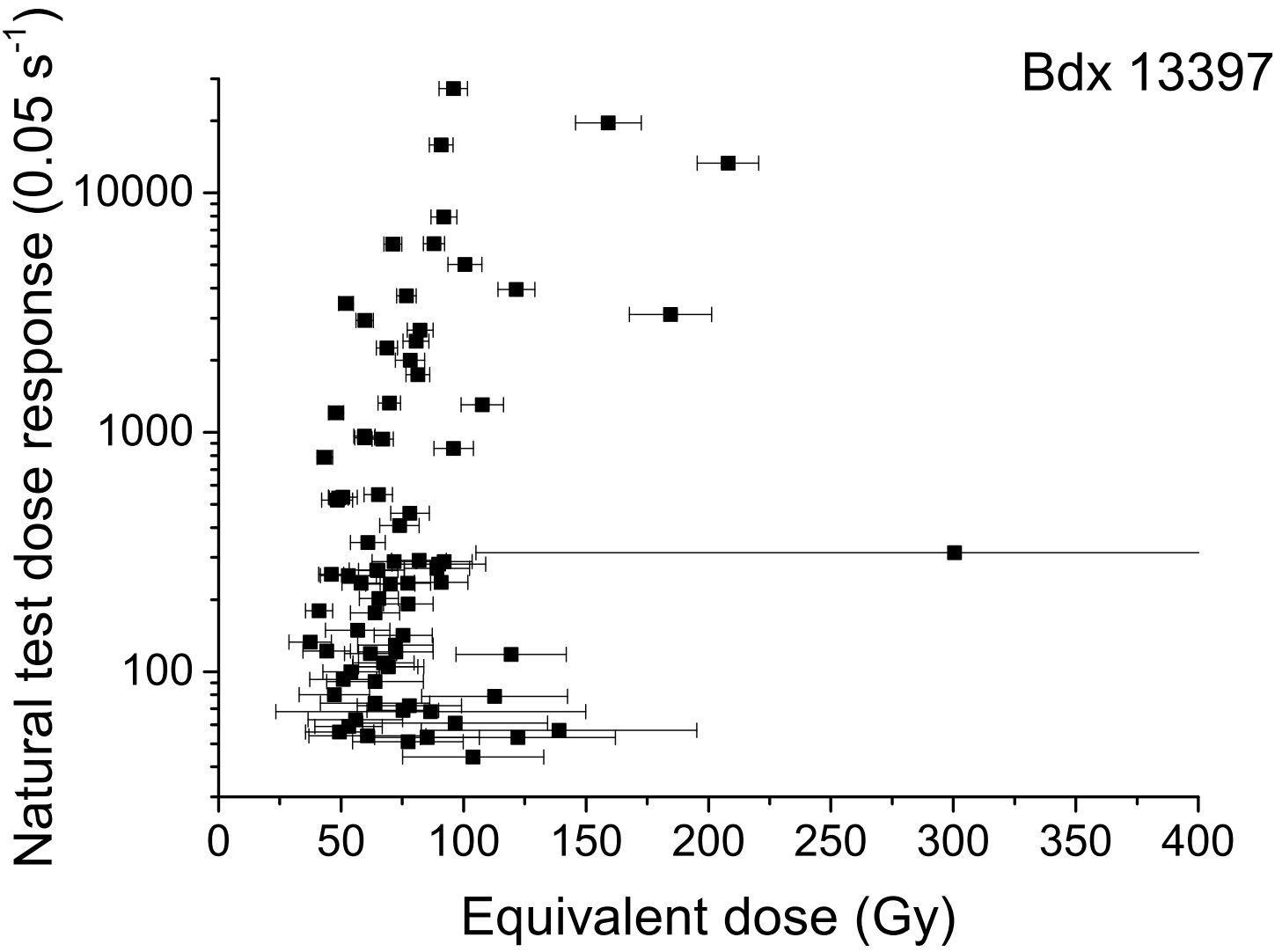

Figure 4 - BottomRight

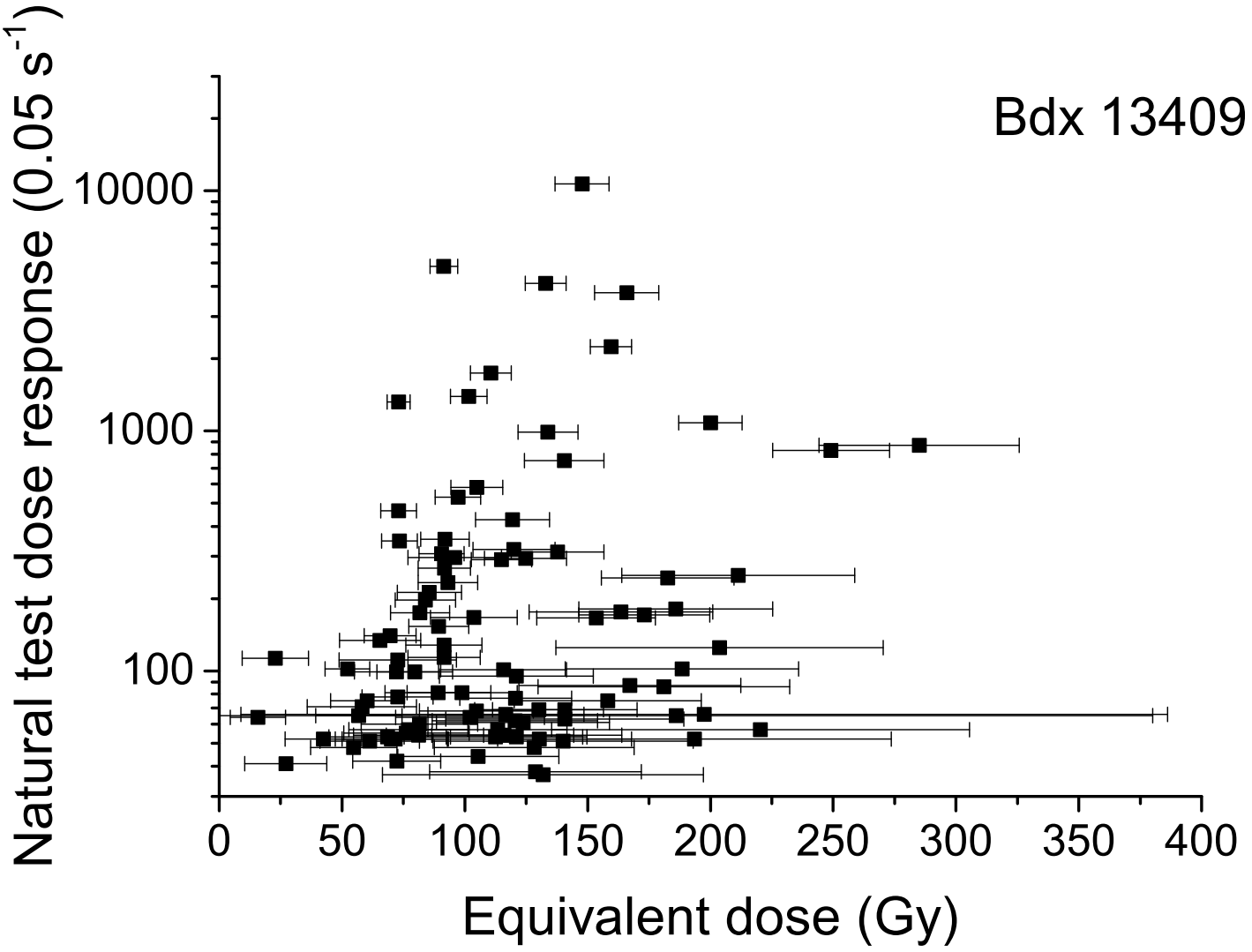

Figure 5 - TopLeft

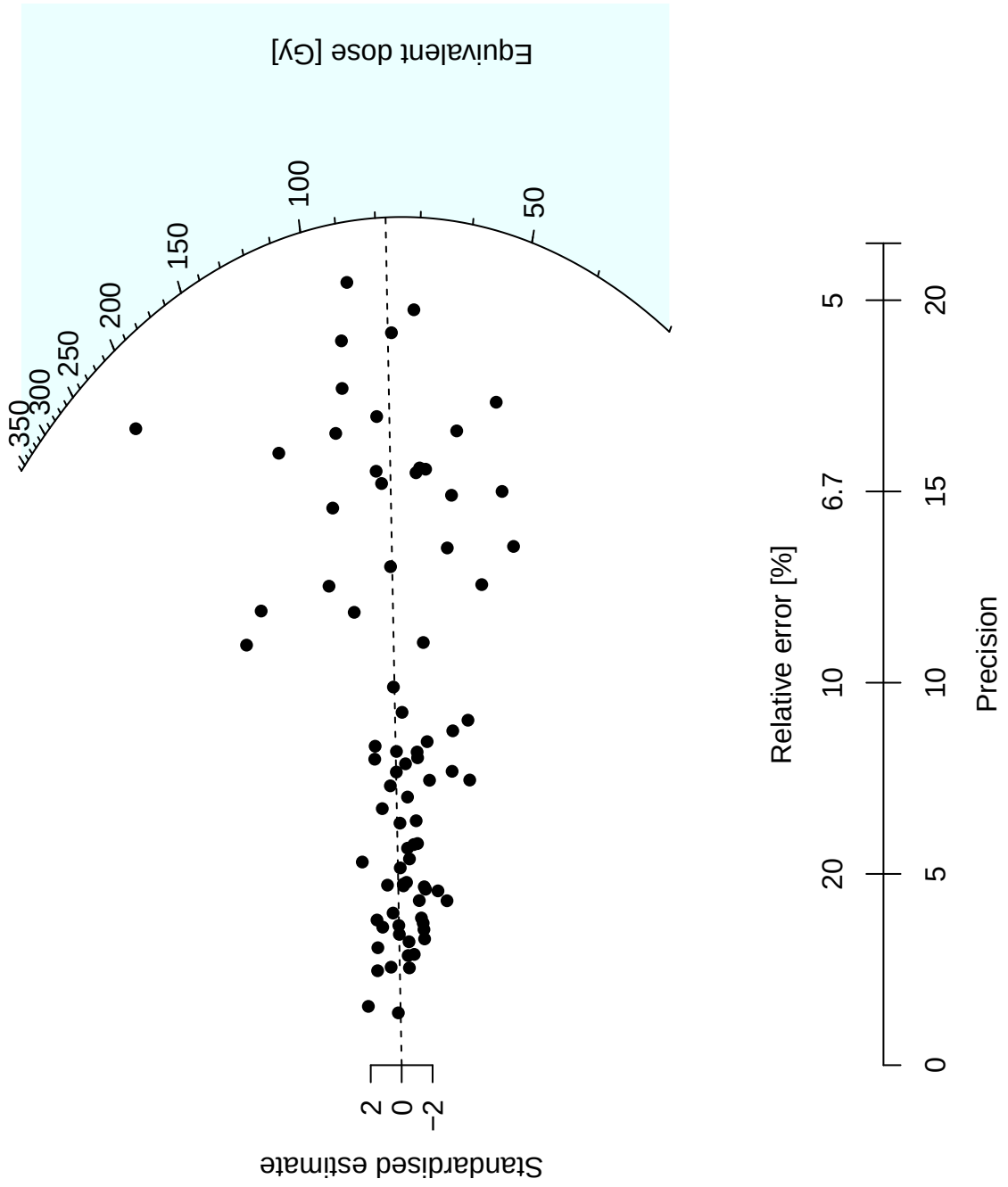

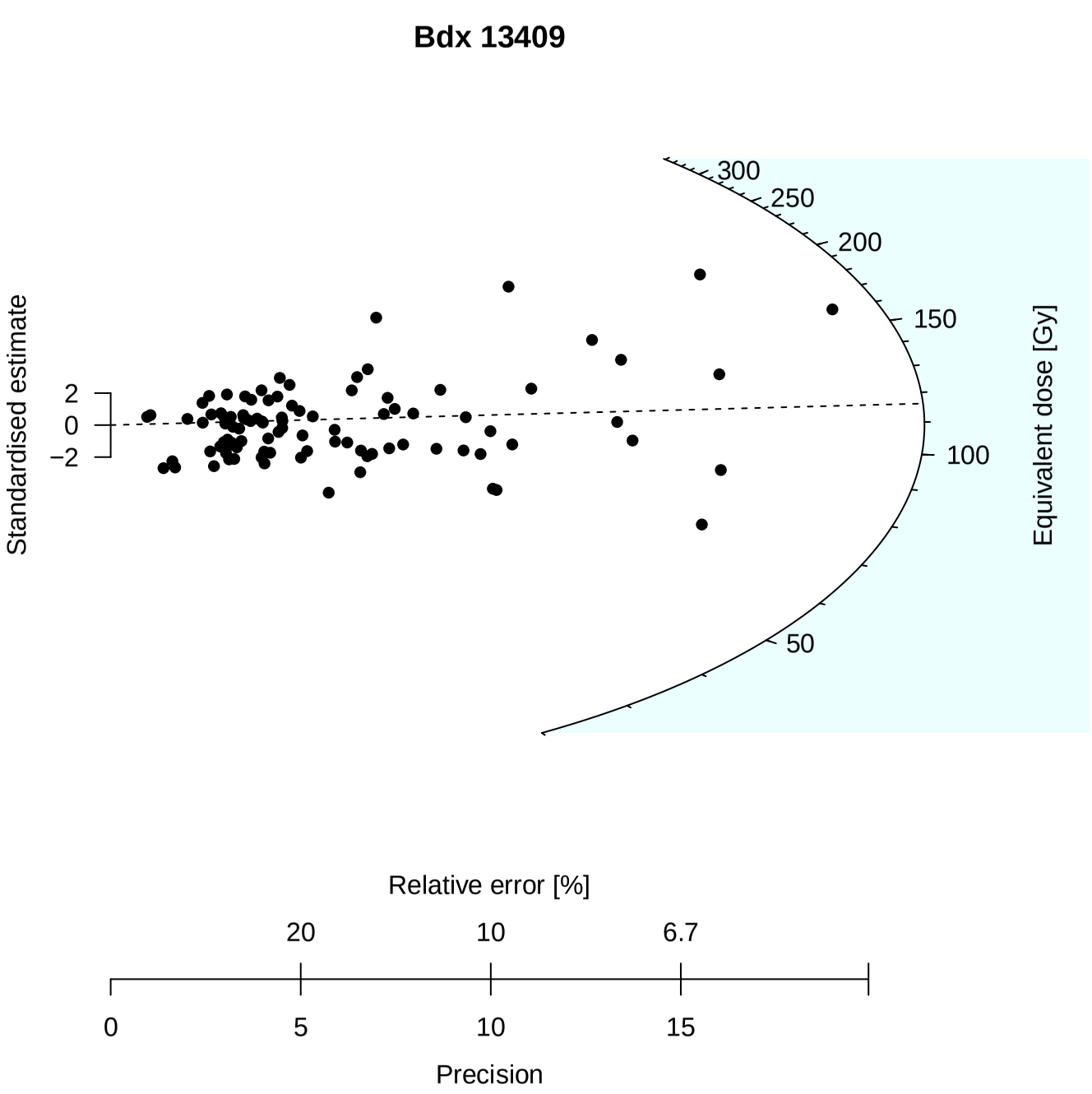

Figure 5 - TopRight

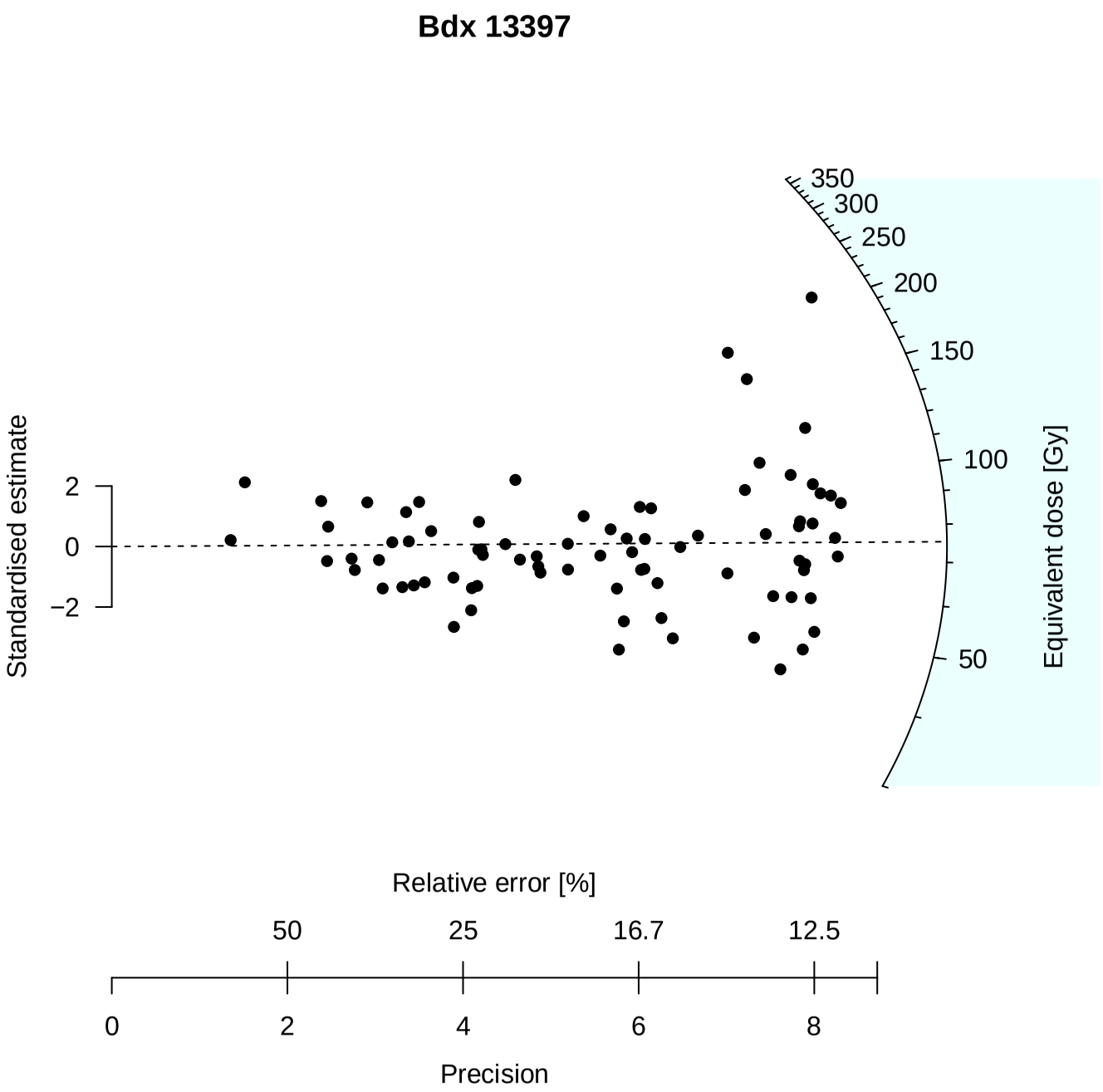

Figure 5 - MiddleLeft

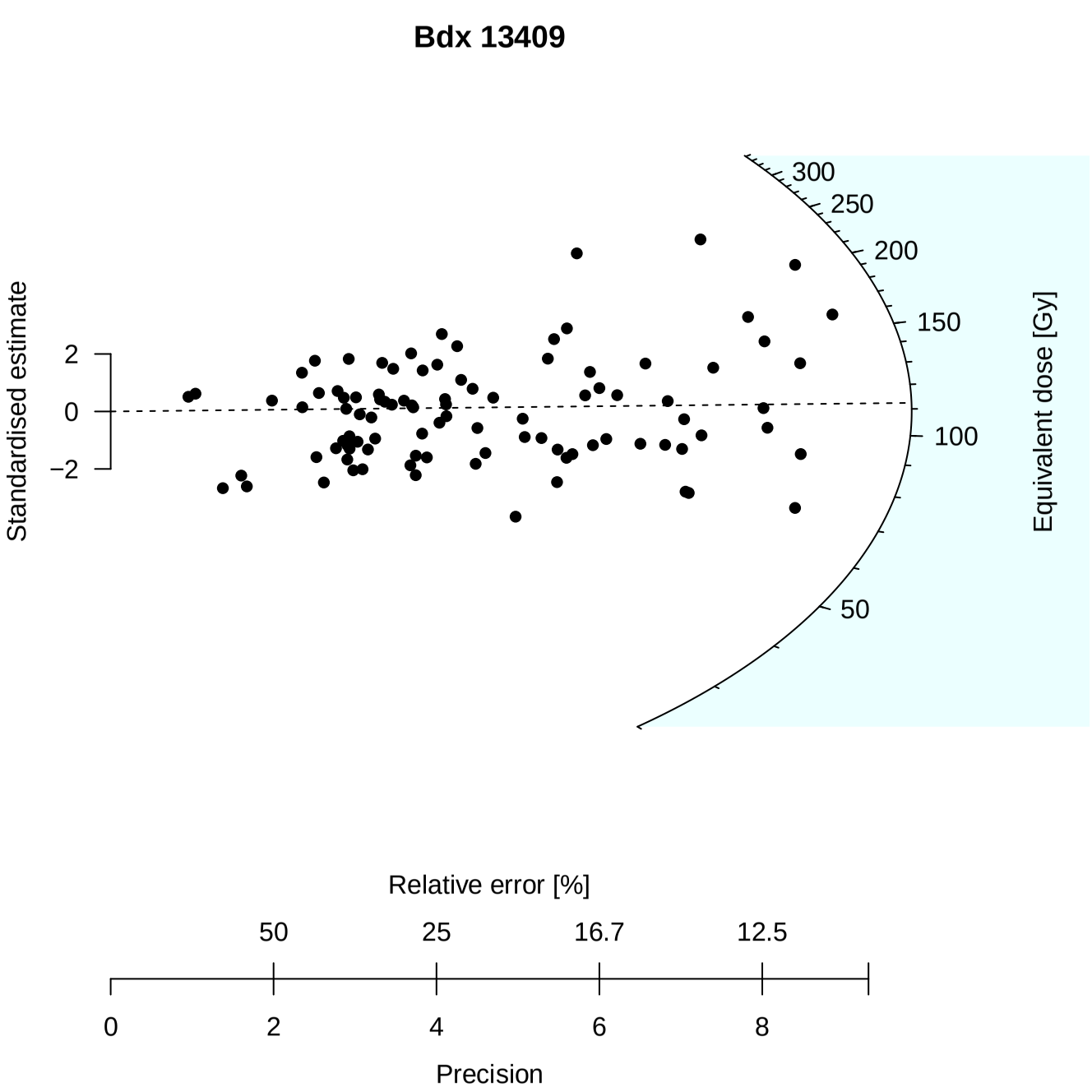

Figure 5 - MiddleRight

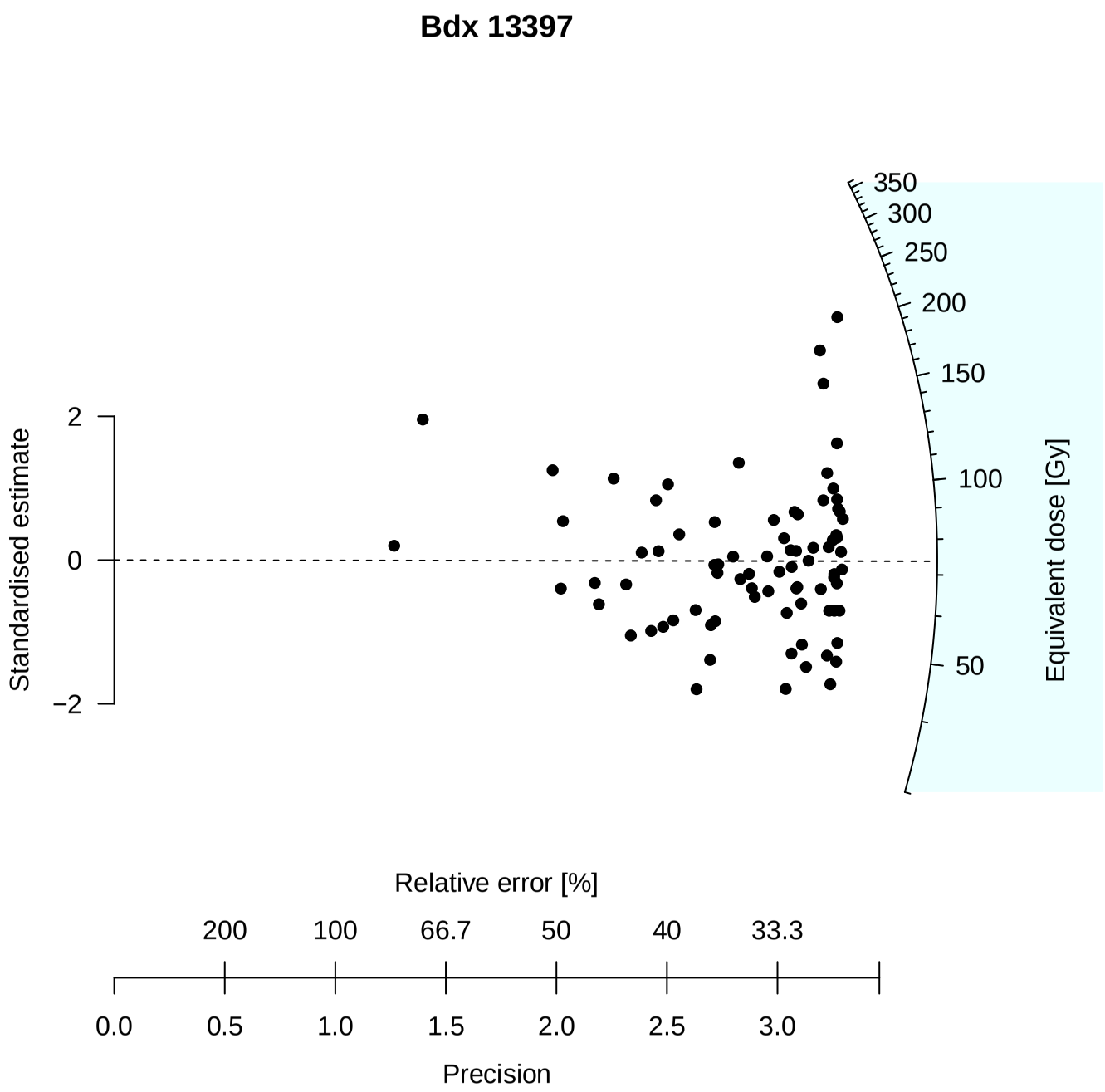

Figure 5 - BottomLeft

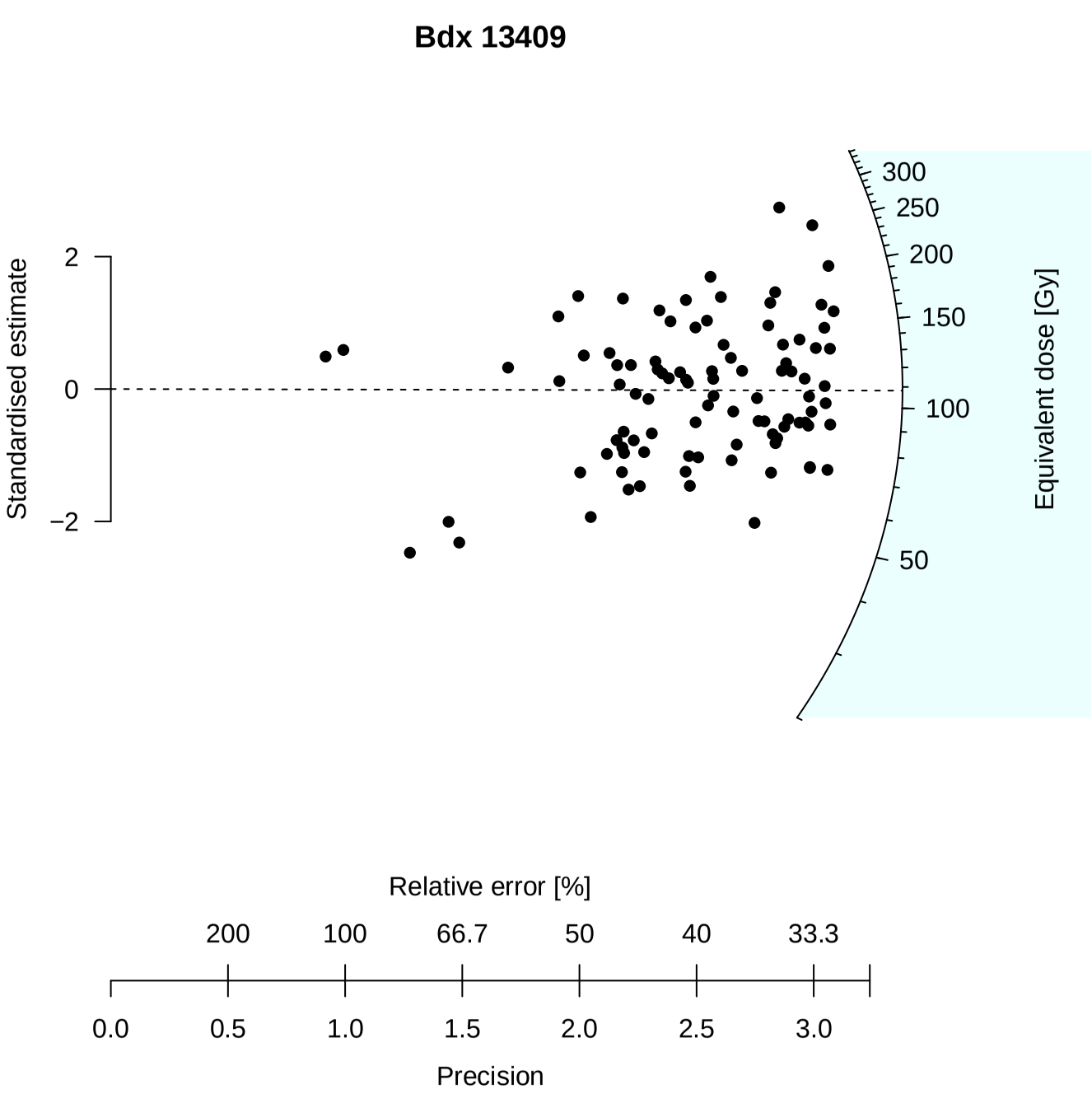

Figure 5 - BottomRight

Figure 6

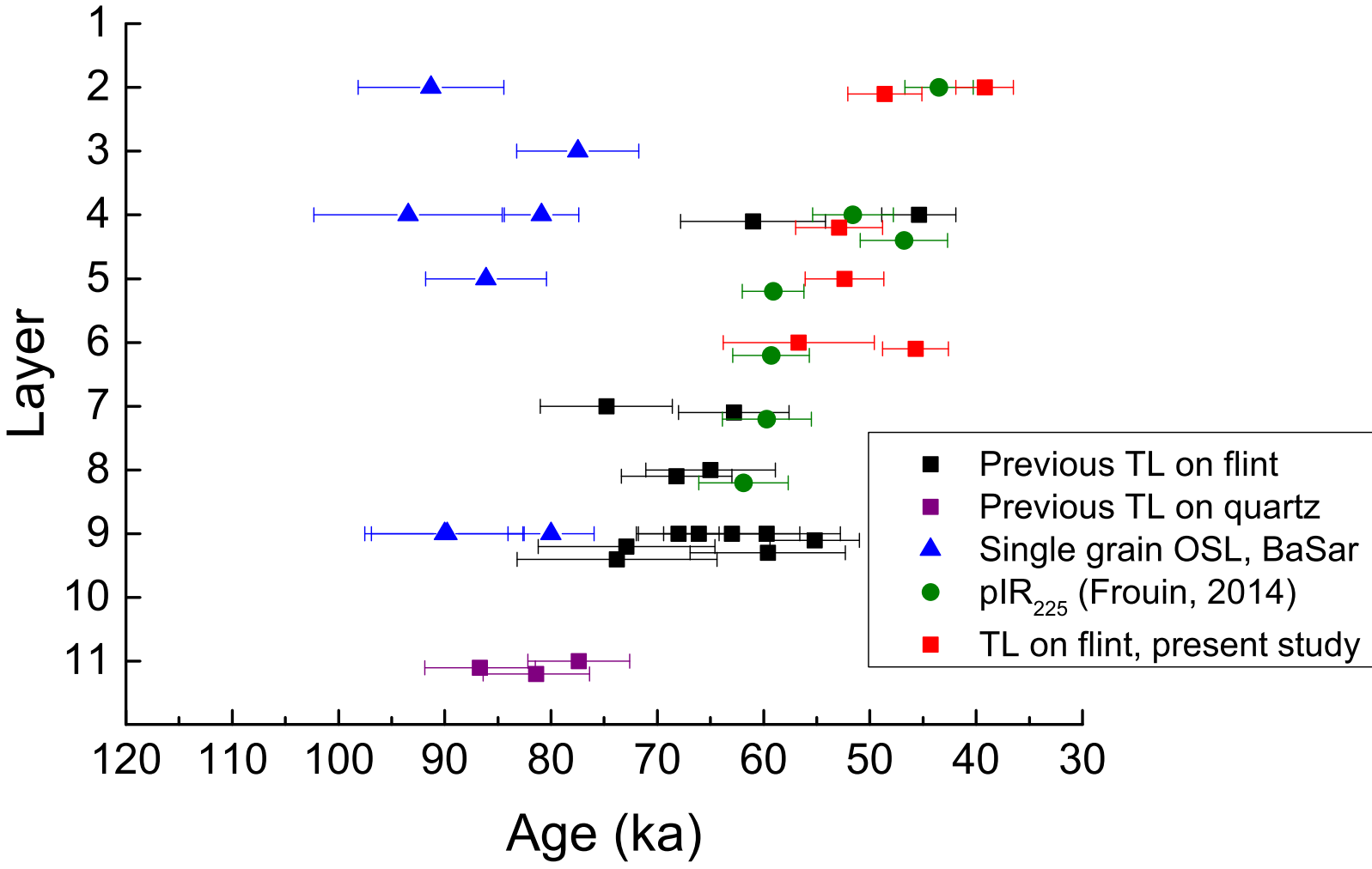
Layer
1
2
3
4
5
6
7
8
9
10
11
120
110
100
90
80
70
60
50
40
30
Age (ka)
Previous TL on flint
Previous TL on quartz
Single grain OSL, BaSar
pIR225 (Frouin, 2014)
TL on flint, present study

Figure 7

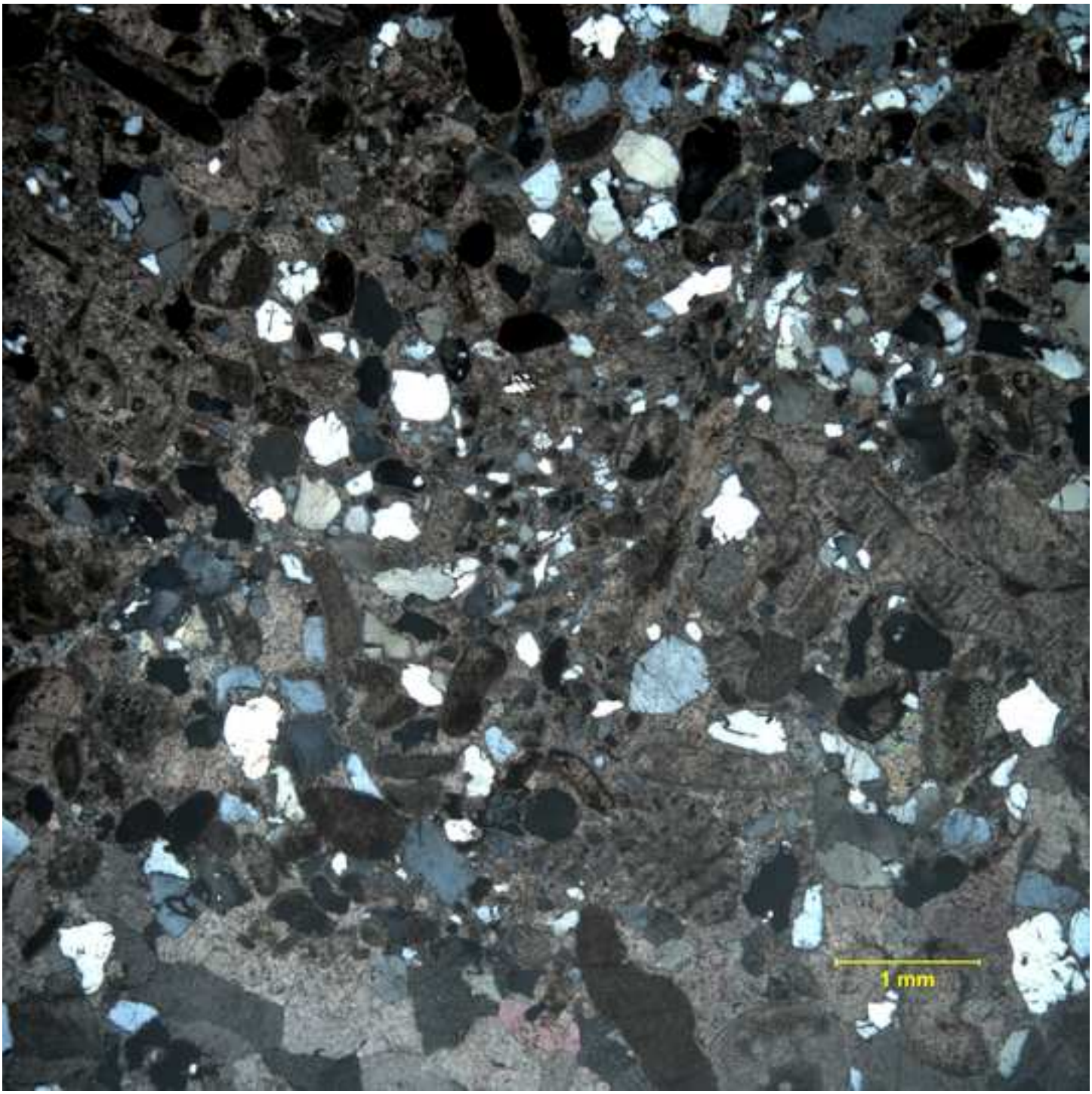

Figure 8

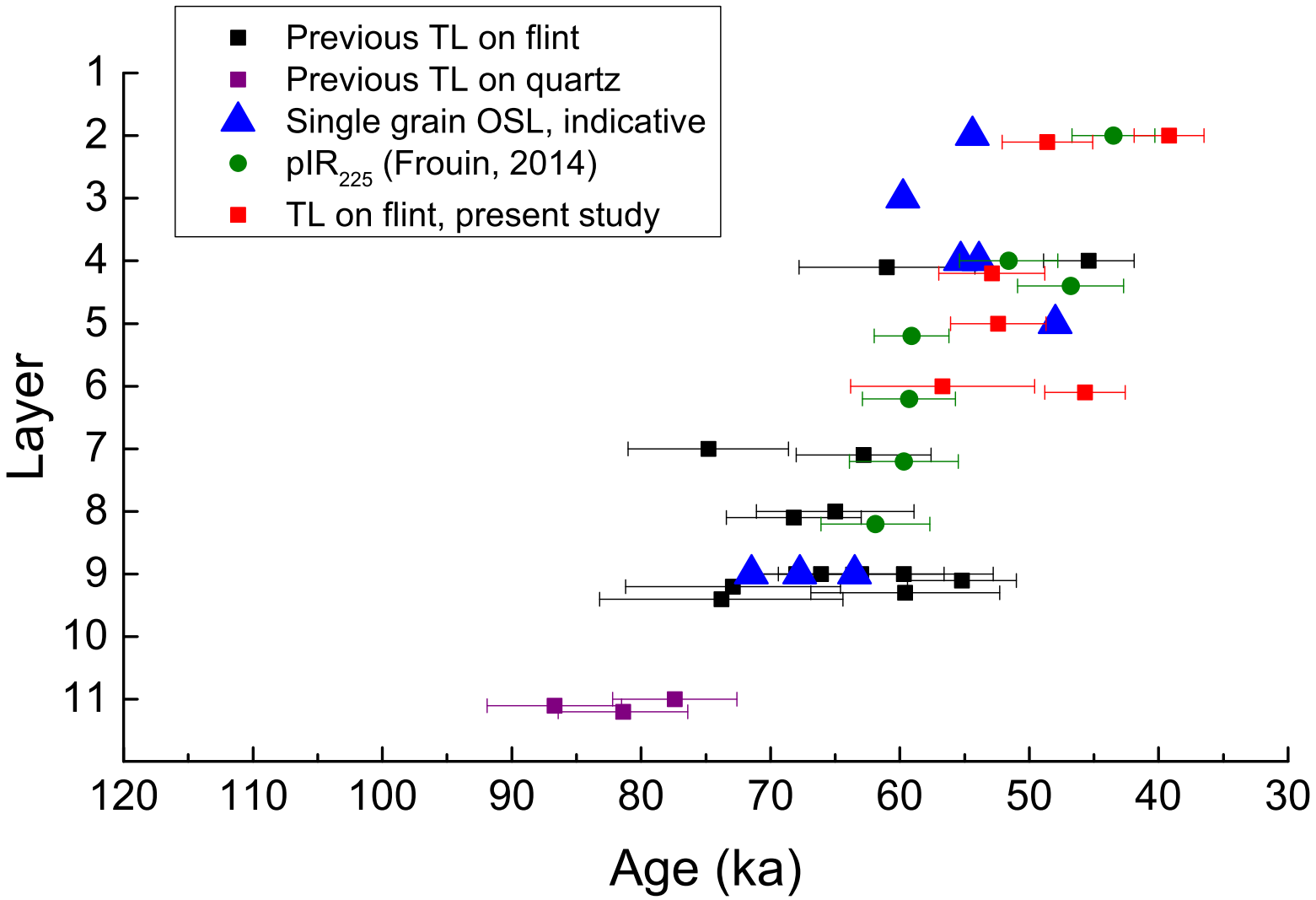
Previous TL on flint
Previous TL on quartz
Single grain OSL, indicative
pIR225 (Frouin, 2014)
TL on flint, present study
Layer
1
2
3
4
5
6
7
8
9
10
11
120
110
100
90
80
70
60
50
40
30
Age (ka)

Table 1

Sample	Layer	K (%)	σ	U (ppm)	σ	Th (ppm)	σ	Alpha dose rate ($Gy.ka^{-1}$)	σ	Beta dose rate ($Gy.ka^{-1}$)	σ	Gamma dose rate ($Gy.ka^{-1}$)	σ	Cosmic dose rate ($Gy.ka^{-1}$)	σ	Total dose rate ($Gy.ka^{-1}$)	σ	D_e (Gy)	σ	Age (ka)	σ
Bdx 16773	2	0.137	0.007	1.37	0.14	0.305	0.031	0.164	0.015	0.315	0.020	0.476	0.050	0.11	0.01	1.065	0.057	41.8	0.4	39.2	2.8
Bdx 16774	2	0.132	0.007	1.58	0.16	0.525	0.053	0.169	0.015	0.348	0.025	0.316	0.033	0.11	0.01	0.944	0.045	45.9	0.8	48.6	3.6
Bdx 16777	4	0.175	0.009	1.61	0.16	0.585	0.059	0.189	0.017	0.388	0.027	0.169	0.017	0.11	0.01	0.857	0.036	45.4	0.6	53.0	4.1
Bdx 16783	5	0.049	0.002	2.15	0.22	0.506	0.051	0.258	0.024	0.365	0.031	0.516	0.050	0.16	0.01	1.300	0.064	65.5	1.1	50.4	3.5
Bdx 16786	6	0.124	0.006	1.15	0.11	0.409	0.040	0.143	0.018	0.276	0.020	0.410	0.042	0.11	0.01	0.940	0.109	53.3	1.0	56.7	4.0
Bdx 16788	6	0.068	0.003	1.03	0.10	0.920	0.092	0.146	0.012	0.229	0.016	0.375	0.037	0.11	0.01	0.860	0.043	39.3	0.5	45.7	3.1

Table 1. TL data. List of samples with their radioelement contents and dosimetry quantities. Alpha dose rates were calculated using an average a-value of 0.05 ± 0.02. Beta and gamma dose rates were corrected for the effect of moisture following Guérin and Mercier (2012); beta dose rate attenuation factors were taken from Guérin et al. (2012). The systematic uncertainty of the laboratory dose rate (2%) was added in quadrature to all age uncertainties.

Table 2

Sample	Layer	K (%)	σ	Effective U (ppm)	σ	Th (ppm)	σ	Gamma dose rate ($Gy.ka^{-1}$)	σ	Beta dose rate ($Gy.ka^{-1}$)	σ	Cosmic dose rate ($Gy.ka^{-1}$)	σ	Total dose rate ($Gy.ka^{-1}$)	σ
13401	2	0.628	0.013	1.62	0.01	7.19	0.10	0.334	0.070	0.702	0.025	0.11	0.02	1.176	0.077
13402	4	0.347	0.010	0.98	0.01	3.89	0.07	0.343	0.070	0.396	0.014	0.11	0.02	0.879	0.074
13408	3	0.364	0.010	1.19	0.02	4.62	0.08	0.450	0.068	0.442	0.015	0.16	0.02	1.082	0.073
13409	4	0.780	0.015	1.93	0.03	9.42	0.11	0.434	0.030	0.873	0.031	0.16	0.02	1.497	0.048
13410	5	0.551	0.012	1.62	0.03	7.75	0.10	0.458	0.068	0.664	0.023	0.16	0.02	1.312	0.075
13394*	9	0.401	0.018	1.7	0.03	9.64	0.11	0.264	0.068	0.613	0.021	0.11	0.02	1.017	0.059
13396*	9	0.279	0.011	1.38	0.03	7.15	0.11	0.352	0.068	0.456	0.015	0.11	0.02	0.948	0.073
13397*	9	0.360	0.016	1.12	0.03	6.28	0.08	0.308	0.030	0.463	0.018	0.16	0.02	0.961	0.041

Table 2. OSL dose rate data (adapted from Guérin et al., 2012). List of samples with their radioelement contents and dosimetry quantities. Effective U takes into account the disequilibrium of U-series at Roc de Marsal (see Guibert et al., 2009; Guérin et al., 2012). Beta and gamma dose rates were corrected for the effect of humidity following Guérin and Mercier (2012); beta dose rate attenuation factors were taken from Guérin et al. (2012). Gamma dose rates were measured in situ using Al_2O_3:C dosimeters.

Note: (*) denotes samples from combustion features, and thus heated in the past.

Table 3

			CDM								UAM				AM-CDM				BaSar				
Sample	Layer	n	D_e (Gy)	σ	OD (%)	σ	UGM D_e (Gy)	σ	UGM/ CDM	Age (ka)	σ	D_e (Gy)	σ	Age (ka)	σ	D_e (Gy)	σ	Age (ka)	σ	n_1	D_e (Gy)	σ	Age (ka)	σ
13401	2	54	99	5	29	4	97	8	0.98	85	7	105	5	89	8	104	6	88	8	196	107	3	91	7
13402	4	40	75	5	37	5	72	8	0.97	85	9	81	6	92	11	80	7	91	11	147	82	3	96	9
13408	3	70	82	4	32	4	81	6	0.98	76	6	88	4	81	7	87	5	80	7	250	84	2	77	6
13409	4	97	108	4	32	3	104	7	0.96	72	4	115	5	77	4	114	6	76	5	324	121	3	81	3
13410	5	74	109	5	37	4	112	8	1.03	83	6	124	7	94	8	116	7	89	8	246	113	3	85	6
13394*	9	47	93	4	26	4	90	6	0.97	91	8	96	5	94	9	96	5	94	9	181	91	2	90	7
13396*	9	41	78	3	21	4	77	5	0.99	82	7	81	4	85	8	80	4	84	8	159	85	2	90	8
13397*	9	81	74	3	30	3	74	5	1.01	77	5	80	4	83	6	77	4	80	5	249	77	2	80	4
Average									0.99±0.01	81	2			87	2			88	2				86	2

Table 3. OSL equivalent doses and ages. 'CDM': Central Dose Model (Galbraith *et al.*, 1999). 'UGM': Unweighted Geometric Mean of individual D_e estimates. 'UGM/CDM': Ratio of Unweighted Geometric Mean to CDM dose estimates. 'UAM': Unweighted Arithmetic Mean (Thomsen *et al.*, 2015). 'AM-CDM': Arithmetic Mean of the CDM (see text for details). 'BaSar': Bayesian Model for SAR analysis (Combès *et al.*, 2015). 'n' is the number of grains for which the uncertainty of the natural test dose signal is less than 20 %, and D_0 > 105 Gy. 'D_e': equivalent dose. The systematic dose rate uncertainty was not included in this D_e estimate, but was incorporated in the final age uncertainties. 'OD (%)': overdispersion parameter as determined with the CDM. 'n_1' is the number of grains for which the uncertainty of the natural test dose signal is less than 20 %. The 'Average' ages are calculated assuming that all samples date the same event, i.e. that the whole stratigraphic sequence was deposited over a short period of time compared to the age uncertainties. However, the quoted standard error of the mean is only indicative, as systematic and random uncertainties have not been treated separately (this would require complex statistical calculations and goes well beyond the scope of this article).

Note: (*) denotes samples from combustion features, and thus samples heated in the past.

Table 4

Sample	Layer	AM-MDM D_e (Gy)	σ	Age (ka)	σ	Indicative age (ka)
13401	2	85	11	72	10	54
13402	4	59	9	67	11	54
13408	3	79	8	73	9	60
13409	4	109	10	73	7	55
13410	5	80	13	61	10	48
13394*	9					68
13396*	9					71
13397*	9					63

Table 4. Minimum quartz OSL ages calculated with the AM-MDM, and 'indicative' quartz OSL ages. AM-MDM ages have been calculated with the MDM model (Galbraith et al., 1999) and modified to the estimate the arithmetic mean of doses (like the AM-CDM dose is deduced from the CDM dose, see section 3.2.1). The 'indicative' ages correspond to ages calculated after modelling the dilution effect due to the presence of $CaCO_3$ in the sediment (see text for details). The samples with a * denote samples heated in the past.